Aalto-yliopisto
Insinööritieteiden
korkeakoulu

Teemu Suksi

Hardness Classification of Rocks Using Spectroscopy

Diplomityö, joka on jätetty opinnäytteenä tarkastettavaksi diplomi-insinöörin tutkintoa varten.

Espoossa 29.8.2017
Valvoja: Professori Jussi Leveinen
Ohjaaja: DI Lasse Kangas

Aalto-yliopisto
Insinööritieteiden
korkeakoulu

Aalto-yliopisto, PL 11000, 00076 AALTO
www.aalto.fi

Diplomityön tiivistelmä

Tekijä Teemu Suksi		
Työn nimi Kivien kovuusluokittelu spektrimenetelmillä		
Koulutusohjelma Rakennus –ja ympäristötekniikka		
Pää-/sivuaine Teknillinen geologia ja sovellettu geofysiikka		**Koodi** IA3029
Työn valvoja Jussi Leveinen		
Työn ohjaaja(t) Lasse Kangas		
Päivämäärä 29.08.2017	**Sivumäärä** 74	**Kieli** Englanti

Tiivistelmä

Perinteisesti kiviaineksia on luokiteltu laboratoriotestein. Nämä testit vaativat useita vaiheita ja voivat usein olla aikaa vieviä. Tämä saattaa johtaa huolimattomuuteen materiaalien valintaprosessissa, millä saattaa olla negatiiviset vaikutukset rakentamisen laatuun.

Tässä työssä tuotiin esiin idea spektroskooppisten menetelmien hyödyntämisestä kiviaineksen kovuus luokittelussa, aikaa vievien laboratoriotestien sijaan. Spektroskooppisten menetelmien on todettu olevan tehokkaita kemiallisten yhdisteiden, eritoten mineraalien, tunnistamisessa. Tämän työn tarkoituksena on viedä tunnistus prosessi astetta pidemmälle, keskittyen mineraaleista kostuvien kappaleiden, kivien, tunnistamiseen.

Työssä käytetyt näytteen koostuivat kahden eri kovuusluokan omaavista kivinäytteistä. Näitä tutkittiin spektroskooppisilla menetelmillä. Spektroskooppiset menetelmät, joilla näytteitä tutkittiin, koostuivat toisiaan tukevista heijastus sekä Raman spektroskopioista. Heijastus spektroskopiaa hyödynnettiin erillisten näytteiden luokitteluun niiden kovuuden perusteella. Raman spektroskopiaa taas käytettiin erilaisten mineralogisten alueiden luokitteluun ja kartoittamiseen näytepinnoista. Näillä menetelmillä kerätty data luokiteltiin erilaisilla luokittelualgoritmeilla. Luokittelualgoritmit jaoteltiin fyysisiin ominaisuuksiin keskittyvään ja statistiseen lähestymistapaan. Statistinen lähestymistapa koostui lähinnä koneoppimiseen nojaavista algoritmeista.

Työn tulokset osoittavat selvästi koneoppimisen ylivertaisuuden perinteisiin fyysisiin ominaisuuksiin keskittyviin algoritmeihin verrattuna. Koneoppimiseen nojaavat algoritmit pärjäsivät huomattavasti paremmin sekä näytteiden luokittelussa että näytepintojen kartoituksessa. Koneoppiminen suoriutui luokittelusta jopa 85 prosentin tarkkuudella, kun taas parhaiten suoriutunut fyysisiin ominaisuuksiin keskittyvä algoritmi saavutti ainoastaan 63 prosentin tarkkuuden. Samankaltainen ilmiö havaittiin myös kartoitusluokittelussa.

Tutkimuksen tuloksena voitiin osoittaa että eri kovuuden omaavia kivinäytteitä voidaan luokitella spektroskooppisia menetelmiä hyödyntäen. Luokittelun onnistuminen riippuu pitkälti käytetyistä luokittelualgoritmeista. Työn päätelmänä todettiin että mitä monimutkaisempi luokittelualgoritmi, sitä tarkempi luokittelun lopputulos.

Avainsanat Raman, heijastuminen, spektroskopia, kiviaines, luokittelu, koneoppiminen

Aalto University
School of Engineering

Aalto University, P.O. BOX 11000, 00076 AALTO
www.aalto.fi

Abstract of master's thesis

Author Teemu Suksi		
Title of thesis Hardness Classification of Rocks Using Spectroscopy		
Degree programme Environmental Engineering		
Major/minor Engineering Geology and Applied Geophysics		**Code** IA3029
Thesis supervisor Jussi Leveinen		
Thesis advisor(s) Lasse Kangas		
Date 29.08.2017	**Number of pages** 74	**Language** English

Abstract

Traditionally, aggregate sources have been classified using laboratory testing. These tests require multiple steps and can often be time consuming. This can lead to negligence in material selection process, which in turn can have a negative impact on the quality of construction.

This thesis presents an idea of using spectroscopic methods in place of the time consuming laboratory tests to classify aggregates based on their hardness. Spectroscopic methods have been shown in the past to be effective in identifying chemical compounds, especially minerals. This thesis intends to take the identification a step further, and concentrate on objects that comprise minerals, i.e. rocks.

Samples used in this thesis consisted of rocks of two different hardness grades. These rock samples were examined using spectroscopic techniques. Complementary spectroscopic techniques; reflectance spectroscopy and Raman spectroscopy, were used to gather data on the samples. Reflectance spectroscopy was used to classify individual rock samples based on their hardness. Raman spectroscopy, on the other hand, was used to classify and map different mineralogical areas on the sample surfaces. The gathered data was classified using different classification algorithms. These algorithms were divided into physically-based and statistical approaches. The statistical approach consisted of mainly machine learning based algorithms.

The results of this thesis clearly indicate the superiority of machine learning algorithms over the traditional physically-based algorithms. Machine learning algorithms performed significantly better in both sample classification and mapping, with the most accurate algorithm reaching a classification accuracy of 85 percent, while the best physically based algorithm could only reach an accuracy of 63 percent. A similar trend was identified with the mapping classification.

The research was able to demonstrate that rock samples of different hardness can be classified using spectroscopy. The success of the classification is largely dependent on the algorithms used to perform the classification. A general conclusion was reached that the more complex the algorithm, the more accurate it is when performing the classification.

Keywords Raman, reflectance, spectroscopy, aggregate, classification, machine learning

Alkusanat

Tämä diplomityö tehtiin osana Challenge Finland-hanketta, Aalto yliopiston toimeksiantona ja Innovaatiorahoituskeskus Tekesin rahoituksella.

Haluan kiittää Teknologian tutkimuskeskuksen Teemu Kääriäistä mahdollisuudesta mittainstrumenttien käyttöön, sekä Seepsula Oy:tä näytteiden tarjoamisesta työtä varten. Lisäksi haluan kiittää Geologian tutkimuskeskuksen Heikki Nurmea avusta näytteiden valintaprosessissa.

Erityiskiitokset haluan osoittaa valvojalleni Jussi Leveiselle ja ohjaajalleni Lasse Kankaalle mahdollisuudesta työn tekemiseen sekä tuesta ja korvaamattomasta avusta työn tekemisessä ja eteenpäin viemisessä. Erityiskiitokset osoitan myös perheelleni ja ystävilleni, jotka osoittivat tukeaan ja mahdollistivat rentoutumisen henkisesti kuormittavinakin aikoina.

Espoo 7.9.2017

Teemu Suksi

Table of Contents

Markings

A_N		Nordic abrasion value
E	[J]	energy of a photon
I		observed intensity
I_0		original light intensity
M_1	[g]	dry mass of test specimen
M_2	[g]	dry mass of aggregate particles greater than 2 mm
R^n		real coordinate space
h	[Js]	Planck's constant
k	[cm^{-1}]	absorption coefficient
m	[g]	mass retained on 1.6 mm sieve
q	[C]	charge of vibration
v	[Hz]	frequency of photon
v_R	[Hz]	frequency of scattered radiation
v_s	[Hz]	frequency of vibration
v_0	[Hz]	frequency of exciting radiation
α	[Cm2/V]	molecular polarizability
ε		strain of material
ρ_p	[Mg/m^3]	pre-dried particle density
σ	[Pa]	normal stress

Abbreviations

ICCD	Intensified charge-coupled device
LIBS	Laser induced breakdown spectroscopy
MIR	Mid-wave infrared
NIR	Near-infrared
OH	Hydroxy group
SAM	Spectral angle mapper
SERS	Surface enhanced Raman scattering
SVM	Support vector machine
VNIR	Visible and near-infrared
XRD	X-ray diffraction

1 Introduction

Rock material serves many purposes in construction. This rock material, also referred to as aggregate, varies in quality. Aggregates must exhibit specific physical, chemical and mechanical properties for each specific end use and it is essential that only the best quality is used in the most challenging applications, e.g. highways.

For years, the quality of the aggregate has been determined by time consuming laboratory tests, where aggregate from quarries is sampled and tested with standardized tests. These laboratory tests can delay the whole construction process and in the worst case scenario this may lead to the usage of too brittle aggregate, which in turn may lead to structural failures.

Rocks are formed by minerals. Minerals are chemical compounds found everywhere in nature. The chemical structure of minerals can vary based on the geological environment where they have been formed. These differences in chemical structure of minerals, and ultimately, rocks, can be studied with the help of spectroscopy. Spectroscopy is, in essence, a non-destructive method to study light and its properties. When an object is illuminated with electromagnetic radiation, i.e. light, an interaction between the object and the radiation occurs. This interaction can then be captured and analyzed with spectroscopic methods.

Minerals have been successfully identified over the years using spectroscopy. The purpose of this research is to take the identification a step further and apply the spectroscopic methods to identify rocks of different composition. The possible application of spectroscopy to rock identification could provide an efficient method of surveying material sources, e.q. quarries, to separate specific areas of interest, without the need for sample preparation. These in-situ measurements could then be used to qualify aggregate from quarry surfaces in place of the time consuming laboratory test, and thus make the material selection process more efficient.

Spectroscopy has been successfully integrated in laser monitoring systems in the past. A method known as Laser Induced Breakdown Spectroscopy (LIBS) has been used to model spectra emission data and this data has then been correlated with aggregate sources and aggregate properties. LIBS technology has been shown to have potential to identify aggregate sources in real-time in the field without sample preparation. (Chesner, McMillan 2012.)

This thesis concentrates on the classification of Finnish aggregate sources. First, in section 1.1 the goal of the research is presented and then in chapter 2, basic information about Finnish bedrock is presented. Then the thesis moves on to the chapter 3, where specific spectroscopic methods used in this research are presented. After the spectroscopy has been discussed, the focus is shifted towards aggregate properties in chapter 4, and then traditional laboratory tests performed on aggregate in chapter 5. These chapters conclude the basic theory of this thesis. In chapter 6 and 7, the research methods used in this thesis and the results achieved with the methods are presented. Lastly, in chapters 8 and 9, the results are discussed and conclusions of the research are given.

1.1 Goal of the Research

The basis of this thesis is the assumption that aggregates could be differentiated into distinct classes based on their hardness, by using spectroscopic techniques. It is hypothesized that based on the spectral properties of minerals and composition of different kinds of rocks, rock samples could be reliably differentiated from each other.

This thesis concentrates on the hardness classification of rocks by using spectroscopy; hence, the main research question can be formulated as follows:

- Can spectroscopy be used to classify different types of rocks based on their hardness?
- What is the best method to classify data into different groups?
- Based on laboratory measurements, could the hardness analysis be applied to field conditions?

The aim of this thesis is to identify a correlation between the data acquired via spectroscopy and the hardness of different rock samples. The identification of a feasible correlation could prove the efficiency of using spectroscopy to qualify different rock samples in laboratory conditions. This knowledge could then be applied to field conditions where rock surfaces could potentially be qualified in quarry environment. The field application could improve the selection process of rock material used in aggregates and other construction materials. By proving the effectiveness of spectroscopic techniques, the time-consuming laboratory tests could possibly be omitted.

This research examines the classification in laboratory environment by using two widely acknowledged, cost efficient and robust spectroscopic methods in material identification. Should future interest for this kind of technology for this specific purpose occur, cost effectiveness and robustness are some of the primary factors to be considered.

2 Finnish Bedrock

The Finnish bedrock forms almost a third of the Fennoscandian shield and can be divided into specific areas. The northern and eastern areas of Finland belong to the Archean bedrock that is dated between 3100 and 2500 million years old. On the other hand, the southern and middle regions of Finland are part of the 1930 to 1800 years old Paleoproterozoic bedrock. Only a small portion of the Finnish bedrock is less than 1800 million years old and the most significant of these formations are the Mesoproterozoic Rapakivi granite formations of southern Finland, which are estimated to be between 1650 to 1540 years old. After the formation of these Rapakivi granite regions, the Finnish bedrock has changed very little. (Lehtinen, Nurmi et al. 1998a.)

Finnish bedrock comprises approximately 45 % plutonic rocks, 40 % clearly metamorphosed rocks and 10 % faintly metamorphosed plutonic rocks (GARDEMEISTER, KAURANNE et al. 1972). More specifically, approximately 53 % of the Finnish bedrock consists of granitoids and 22 % of migmatites. Only a minor portion of the bedrock is comprised of igneous rock, schist, quartzite and limestone. The northern area of Finland is home to more volcanic rock than the rest of Finland. (Lehtinen, Nurmi et al. 1998a.)

Bedrock is a vital part of engineering. The engineering properties of the bedrock are affected not only by the prescribed petrological properties but also by the structural or tectonic nature of the bedrock. The outer layer of the earth's crust has experienced many kinds of stresses throughout its existence. These stresses have resulted in formation of schistose rocks, folding, faulting, deformation and dislocation of bedrock sections. Additionally, the stresses have resulted in complete alteration of the original petrological features. (GARDEMEISTER, KAURANNE et al. 1972.)

2.1 Introduction to Minerals

The bedrock consists of crystalline chemical compounds. These compounds are called minerals. Oxygen, silicon, aluminum, iron, calcium, magnesium, potassium and sodium are the eight main chemical elements found on earth and together they form up to 99 % of the bedrock material. These elements often appear as silicates, which comprise the most common group of rock forming minerals. (GARDEMEISTER, KAURANNE et al. 1972.)

Minerals consist of atoms (i.e. ions) that have precisely specified molecular locations and spatial arrangement. The structure of the mineral lattice (growth, symmetry and cleaving tendency) depends on the charge, size and bond of the ions. Silicon is capable of forming long chains and depending on how the chains are connected, different silicate groups are formed. The following classification of silicates is used, from toughest structure to the weakest: nesosilicates or orthosilicates (e.g. garnets), inosilicates or chain silicates (pyroxene group e.g. diopside), double chain silicates (amphibole group e.g. hornblende), phyllosilicates or sheet silicates (e.g. mica group) and tectosilicates or "framework silicates" (e.g. feldspars). (Pidwirny 2006.) The average mineral composition of rocks found in the earth's crust is approximately the following: feldspar family 60 %, amphibole and pyroxene groups 17 %, quartz 12 %, others 7 % and mica 4 % (GARDEMEISTER, KAURANNE et al. 1972).

2.2 Introduction to Rocks

Rocks are formed by crystalline mineral grains and consequently, classified based on their mineral composition and structure. These attributes are a consequence of the states which the rock has been through. Every rock has a specified mineral composition, grain size, shape and orientation. These attributes may be consistent throughout the rock in which case the rock is referred to as homogeneous. If the attributes are inconsistent throughout the rock, the rock is referred to as heterogeneous. Sometimes the attributes change periodically and larger areas can be considered homogeneous. (SFS-EN ISO 14689-1:2003.)

The structure of the rock is also characterized by its grain size. Rocks can be classified into six classes based on their grain size. These classes are glassy or amorphous, very fine grained, fine grained, mid-grained, coarse grained and large grained. If the mineral structure of the rock has scattered mineral grains which are larger than average, the rock is referred to as porphyry or mixed-grained. A rock can also be homogeneous or non-homogeneous based on its grain size. The smaller the grain size of the rock, the more it has cohesion surface. Based on laboratory experiments, the strength of a porphyry rock depends on the strength of the scattered mineral grains. If the mineral grains of the rock are isometric, i.e. they are of uniform length to every direction; the rock is referred to as isotropic. When the mineral grains are organized so that they are of constant length to one specific direction, the rock is referred to as anisotropic. Anisotropic rocks are often weaker than isotropic rocks. Generally, it can be said that the flakier the rock, the weaker the rock. (de Vallejo, Luis I González, Ferrer 2011.)

3 Spectroscopy

Light, or electromagnetic radiation, is present everywhere in our daily lives and it constantly interacts with matter in different states. This interaction can have many forms, for example scattering, absorption or reflection. When light encounters a material grain, it can move through the grain, be absorbed by the grain or be reflected from the grain. A portion of the light, or radiation, that a material is subjected to, will always scatter from the material grains. This scattered light can then be detected, captured and measured. The study of this captured light is generally referred to as spectroscopy. (Clark 1995.)

Spectroscopy can be applied to large number of analytical problems faced in the world of science. Spectroscopy as a whole consists of many different methods that differ from each other in not only the used region of electromagnetic spectrum, but also in the nature of interaction to be analyzed and the scale of the analysis, e.g. molecular vs. atomic spectroscopy. The regions of interest in spectroscopy can be for example visible, infrared or ultraviolet ranges of electromagnetic spectrum, and the interaction to be measured can be for example absorption, emission, diffraction or scattering. (Penner 2010.) Different materials have different types of interaction with light. Spectroscopic methods concentrate on evaluating and discriminating these interactions to separate different material from each other. (Hunt 1977.) This research mainly concentrates on the absorption and scattering interactions in Raman and near-infrared spectroscopy, also referred to as reflectance spectroscopy.

Different spectroscopic methods are widely used in both quantitative and qualitative analyses due to the variety of information to be gathered with spectroscopic methods. Absorption spectroscopy methods in the near-infrared and mid-infrared regions have been widely used in the analysis of inorganic compounds, such as minerals and rock faces. (Penner 2010.) When it comes to quantitative analysis of vibrational spectra, absorption spectroscopy behaves largely differently than the inelastic scattering based spectroscopy, i.e. Raman spectroscopy. While the absorption techniques follow Beer's law, the Raman intensity is directly proportional to the concentration of the sample of interest. (Siesler, Ozaki et al. 2008.) Table 1 provides an overview the general methods used in this research.

Table 1. An overview of Raman and Near-Infrared Spectroscopy (Adapted from Siesler, Ozaki et al. 2008).

Method	Type of Vibration	Interaction	Radiation Source	Focus of Study
Raman	Fundamentals	Inelastic scattering	Monochromatic	Scattered radiation
NIR	Overtones, Combinations	Absorption	Polychromatic	Absorbed radiation

An important aspect to consider when a method is applied to industrial use is the sample preparation needed for the conduction of measurements. This aspect is what sets Raman spectroscopy and NIR spectroscopy apart from another rather popular spectroscopic method, MIR spectroscopy, or mid-wave infrared spectroscopy. Raman and NIR spectroscopy require little to no sample preparation, whereas the MIR spectroscopy generally requires specific sample preparation procedures before measurements can be conducted. (Siesler, Ozaki et al. 2008.)

Commonly used distinctions of the regions residing within infrared range of electromagnetic spectrum, as well as the range of visible light, are presented in table 2. It must be noted that the NIR spectroscopy used in this research covers not only the near-infrared region but also a significant portion of what is classified as the short-wave infrared region.

Table 2. The wavelength distinctions of visible and infrared regions of the electromagnetic spectrum.

Region	Wavelength(μm)
Visible or VIS	0.4 - 0.8
Near-Infrared or NIR	0.8 - 1.4
Short-wave infrared or SWIR	1.4 - 3.0
Mid-wave infrared or MIR	3.0 - 8.0
Long-wave infrared or LWIR	8.0 - 15
Far-infrared or FIR	15 - 1000

The following sections describe the spectral methods used in this research, namely reflectance spectroscopy and Raman spectroscopy, in more detail. First, basics of reflectance spectroscopy are discussed, and then the basic principles of Raman spectroscopy are presented. Lastly, the spectral properties of materials affecting the reflectance and Raman spectrum are discussed.

3.1 Reflectance Spectroscopy

Matter can absorb light photons as a result of many different physical processes. These processes allow for the analysis of the chemical composition of the matter from its reflected radiation. The radiation is modified by the interaction with matter, and the properties of the reflected portion of this radiation are highly dependent on wavelength. (Clark 1995) The reflected radiation contains features that can be detected in different regions of the electromagnetic spectrum. These features are caused by vibrational and electronic processes and appear in the form of slopes and bands in the structure of a spectrum. The vibrational and electronic processes are generated by various elements and compounds in the radiated matter, e.g. hydroxyl groups or iron. (Hunt 1977.)

The reflectance techniques used in this research concentrated on the visible and infrared, or more specifically near-infrared, regions of the electromagnetic spectrum. Common applications for infrared spectroscopy concentrate on the identification of organic matter, although the spectra of inorganic matter have also been widely documented throughout the years. This research concentrates more on the inorganic domain of the infrared spectroscopy due to the inorganic nature of minerals and rocks. A clear distinction between organic and inorganic compounds can be made based on their infrared spectra. The bands that appear in the infrared spectra of organic compounds are generally slimmer and more abundant in numbers than those in the inorganic compounds. The bands in inorganic materials also appear at lower wavelengths than those in the organic materials. (Stuart 2005.)

In the last decade, improvements in optical technology have enabled the transfer of near infrared energy and information. The near-infrared, or NIR, region exhibits absorption bands relating to overtones and combinations of fundamental vibrations of hydrogen and three different elements; carbon, nitrogen and oxygen. The light hydrogen atoms cause these vibrations to be largely anharmonic. The overtones and combinations of vibrations are generally significantly weaker than the fundamental absorption bands, which enables the analysis of thicker samples. (Bokobza 1998.) These vibrations are discussed in more detail in the following sections.

The interpretation of NIR spectra can often be ambiguous due to the nature of the spectral bands they contain. While, for example mid-IR spectra generally contain sharp and narrow absorption features related to the fundamental modes, the NIR spectra exhibits broad features, which are often combinations of many different individual features. This, together with the possible presence of Fermi resonances, can make accurate analysis of band configurations nearly impossible, often limiting the practical usefulness of the NIR region. These problems have however been gradually diminished with the evolution of statistical methods. (Bokobza 1998.) Fast analyzing speed, lack of sample preparation, non-destructive nature of the method and the wide variety of possible samples can be listed among some of the advantages of NIR spectroscopy.

3.1.1 Absorption Processes

Photons are absorbed according to the following Beer's Law, when they enter a medium:

$$I = I_0 e^{-kx} \tag{1}$$

where I is the observed intensity [-]
I_0 is the original light intensity [-]
k is the absorption coefficient [cm^{-1}]
x is the distance travelled through the medium [cm] (Clark 1995).

The basic equation of Beer's law applies only to a single wavelength, and for every wavelength, the absorption coefficient is different. This leads to the variation of the observed intensity, which means that the absorption coefficient as a function of wavelength plays a key role in the analysis of the interaction between photons and matter. (Clark 1995.)

The region of electromagnetic spectrum, which is referred to as VNIR region, or visible and near-infrared region, is home to wide variety of electronic processes. The processes are caused by transitions between energy states inhabited by isolated atoms and ions. These transitions are brought about by changes from one energy state to another, and the by-product of these changes is the absorption or emission of specific wavelengths of electromagnetic radiation. (Hunt 1977.)

When atoms exist in a material in its solid state, the electrons of these atoms can be shared by the whole material, leading to a situation where electrons are not associated with any particular atom. This in turn means that atoms do not exist in individual minerals, and the atoms where the electrons originate from become ions when changes in energy levels occur. These values are referred to as the "energy bands" of the solid. The

electrons that stay bound to the resultant ions have distinct energy states associated with them. The energy levels of ions in elements can be determined by deep lying electrons, or non-shielded outermost electrons. When non-shielded electrons come into contact with electrostatic fields, the fields can greatly influence the electrons. These fields are also referred to as crystal fields, and they originate from negatively charged anions and dipolar groups, or "ligands", surrounding the ions. The properties of these ligands determine the changes induced in the ion. (Hunt 1977.)

For example, iron constitutes for a large number of electronic features found in the VNIR spectra of minerals and rocks. When transition elements, such as iron, located in a solid material encounter a crystal field, their energy levels are different. The different energy levels of the element and the crystal field cause a split to occur, and the energy levels displace into different locations. Crystal fields possess a wide variety of energy level arrangements, and these arrangements can cause the formation of different spectra for a given ion. The arrangements produce spectral features based on the electron spin of the states, with the most prominent features occurring when the spins between the states are the same. On the other hand, when the spins of the states are varied, very weak features, or no features at all, are produced. (Hunt 1977.)

Charge-transfer is a process that occurs when absorbed energy causes an electron to travel between adjacent ions or between ions and ligands (Hunt 1977). The absorption bands caused by these charge-transfers are essential in mineral identification (Clark 1995). The electron that has been influenced to travel between positions is localized in its new position and it does not participate in the conduction band. When localized charge-transfers occur in crystal structures, the electrons can be excited to travel between a ligand orbital and an orbital localized on a central metal ion. Essentially, the charge-transfer produces much more prominent features in the absorption spectra than the crystal field transitions of states with the same electron spin. (Burns 1993.)

Some spectral features can appear in the visible range of electromagnetic spectra with no clear explanation. The electronic phenomenon that causes these features is called "color center". The phenomenon is known to manifest itself in a limited number of colored minerals. The yellow, purple and blue colors of mineral fluorite can be attributed to this phenomenon. (Hunt 1977.)

Real crystals and ideal crystals have very different behavior patterns. Ideal crystals are often immune to effects of radiation, largely due to their completely periodic field potential. Real crystals, however, exhibit lattice defects that disturb the periodicity, i.e. their field potential is not completely periodic. When radiated, the excited electrons of a real crystal do not return to their original positions but instead may become bound to the lattice defects, causing the crystal structure to transform based on the position change of the electrons. (Hunt 1977.)

In some periodic lattices, the close proximity of the ions causes the energy levels of their outer shell electrons to overlap, forming an energy band. This means that electrons have the possibility of existing in two different energy bands, a higher energy band also referred to as "conduction" band, or a lower energy band also referred to as "valence" band. The electrons of the conduction band can wander freely throughout the crystal lattice due to the high energy they possess, whereas valence electrons stay attached to specific bonds and ions. Between these two bands lies a third band that largely determines the materials conductive capabilities. This third band is generally referred to as

"forbidden" band, and while dielectric materials generally have substantial forbidden bands, great conductors, such as metals, generally have almost nonexistent forbidden band. In dielectric materials, valence electrons are generally so tightly bound that large amounts of energy are required to set them free. (Hunt 1977.)

In semiconductors, the energies of the forbidden band and the photons of the electromagnetic radiation merge, resulting in a spectrum that is a step function. An example of this is the yellow of sulfur, which is a result of this kind of step function (Clark 1995). The semiconductors exhibit an intense absorption edge in the VNIR region and the sharpness of this absorption edge is defined by the purity and crystallinity of the material, with pure single crystals often exhibiting steeper absorption edges than non-pure crystals (Hunt 1977).

Energy of a given electronic state can be expressed with equation 2. The equation describes the relation between the electromagnetic radiation and the absorption capabilities of a molecule. According to quantum mechanics, a molecule can absorb a quantum of energy hv, when it is excited with electromagnetic radiation. The frequency of the photon, v, then indicates the location of the specific absorption in the spectrum of the remaining radiation that can then be captured. (Schrader, Bougeard et al. 1995.)

$$E_i = h * v \left(n + \frac{1}{2}\right),\ n = 0,1,2,\ldots \quad (2)$$

where E_i is the energy of a given state [J]
h is Planck's constant [Js]
v is the frequency of the photon [Hz]
n is the vibrational quantum number [-] (Schrader, Bougeard et al. 1995).

The bonds of a crystal lattice can be described by a simple spring analogy. The bonds behave like a spring that has been loaded with weights that enable the whole system to move in vibrational pattern. (Clark 1995.) The motions of a vibrating system are generated by normal modes, also referred to as fundamentals. These fundamentals are simple motions that are restricted in number, and their properties are determined by three distinct atomic features in a material. These features are the attributes of the constituent atoms, their spatial geometry, and the magnitude of binding forces between them. (Hunt 1977.)

When a fundamental mode is excited with multiple quanta of energy, a phenomenon referred to as "overtone" occurs. This phenomenon produces a spectral band at the given multiple of the fundamental frequency, and if several of these phenomena occur simultaneously, the band appears located at the sum of all the frequencies. This sum of frequencies is called a combination tone. (Hunt 1977.) Generally, a molecule can only exhibit vibrational absorptions when it shows a dipole moment, and higher overtones are always weaker than previous overtones (Clark 1995).

The features observed in the NIR region are almost solely caused by overtones and combinations of groups possessing very high fundamental frequencies. The most important of these groups is the hydroxyl group, which appears most frequently in the spectra of terrestrial materials due to the presence of water. Water may appear in many forms and locations in crystal structure, with some of the locations being essential to mineral structure, as for example in gypsum, and some being non-essential as in zeo-

lites. This leads to a large variance in the intensity of features caused by the presence of water. The presence of water can, however, always be diagnosed by two constant features that appear at wavelengths of 1.4 μm and 1.9 μm. (Hunt 1977.)

The cause for the abundance of overtones and combinations and lack of intense fundamental absorptions lies in the fact that most of the hydrogen based fundamentals absorb at higher wavenumbers than the polar groups. This means that the first overtones of hydrogen based fundamentals already appear in the NIR range of electromagnetic spectrum, whereas the more intense fundamental absorptions caused by polar groups appear in the MIR region, and have already lost most of their intensity by the time they reach the NIR region. (Siesler, Ozaki et al. 2008.)

The hydroxyl group has only one fundamental stretching mode that always produces a feature at the wavelength of 2.75 μm. Apart from the fundamental stretching mode, features in the NIR region may also be caused by the first overtone of the hydroxyl stretch, a combination band between hydroxyl group and aluminum or magnesium, or a combination of hydroxyl stretch and a liberated mode. (Hunt 1977.)

Fundamental stretching mode of the hydroxyl group usually creates paired combination bands in the further regions of NIR spectroscopy range, with the exact location being dependent on the presences of either aluminum or magnesium. Carbonates, on the other hand, are responsible for five very distinct bands in the NIR region, which are generated by internal vibrations occurring in a carbonate ion. These features appear in the wavelength ranges of 1.6 to 2.5 μm with the features appearing in the longer wavelength regions being considerably more intense. The origin of different spectral bands can usually be deciphered from their resolution. Vibrational processes tend to create spectral bands that are much sharper in nature and typically occur as multiples, whereas electronic processes tend to create broad single or double bands. (Hunt 1977.)

3.1.2 Reflectance Spectrum

The absorption features in a spectrum generally consist of continuum and individual features. Continuum features are shapes which continue through a large portion of a spectrum and give it its distinctive overall look. Individual features, on the other hand, are features that cause distinct shapes at only specific wavelengths. An example of these features can be seen in figure 1, where a continuum feature gives the spectrum a distinct shape and individual features (sharp indentations) appear superimposed on the continuum feature. (Clark 1995.)

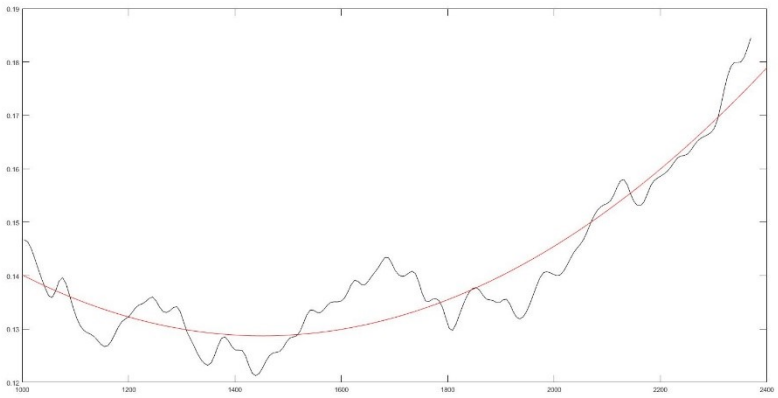

Figure 1. A spectrum where the continuum feature is illustrated by a red trend.

3.2 Raman Spectroscopy

Raman spectroscopy is based on the molecular vibrations caused by changes in the polarizability of molecules. Essentially, Raman spectroscopy explores the Raman scattering originating from an object when it is excited with monochromatic light.

Raman spectroscopy and infrared spectroscopy can be considered complimentary techniques, with both performing slightly different roles in the field of spectroscopy. The complimentary aspect of these techniques can be seen in the fact that some vibrations can only be witnessed with infrared spectroscopy, whereas some can only be witnessed with Raman spectroscopy. Generally the features that appear prominently in infrared spectra are weak in the Raman spectra, and vice versa. Infrared spectroscopy has been traditionally used in industrial applications, whereas Raman spectroscopy has been restricted to laboratory measurements. This distinct separation has formed mainly because of fluorescence. (Schrader, Bougeard et al. 1995.)

Fluorescence is a phenomenon which consists of an atom absorbing a photon to reach an excited energy level. After the atom has reached the excited level, it drops back to the ground level in distinct steps and simultaneously emits two or more photons of smaller energy and longer wavelength. A good example of this is the electric discharge in a fluorescent tube. The electric discharge in the tube reacts with the mercury vapor inside the tube and causes it to emit ultraviolet radiation. The radiation is then absorbed by the atoms of the coating located on the inside of the tube. After the absorption process, the atoms of the coating re-emit light in the longer wavelength portion of the visible range of the electromagnetic spectrum. (Young, Freedman 2004.)

It is important to consider the fluorescence effect in Raman spectroscopy due to the ability of fluorescence to completely mask Raman spectra in the visible region. The effect of fluorescence is approximately one million times more prominent than the Raman Effect. It should be noted however, that fluorescence does not produce effects in the NIR region. This has contributed to the use Raman spectroscopy in conjunction with infrared spectroscopy in material studies. (Schrader, Bougeard et al. 1995.)

The basic Raman spectroscopy is a surface scattering technique that captures and visualizes information based on Raman scattering from molecules on the surface of material. The technique is particularly useful for the analysis of single crystal surfaces and applications, e.g. mineral analysis. Other more advanced Raman techniques include surface-enhanced Raman scattering or SERS, integrated optical waveguide Raman spectroscopy, total internal reflection spectroscopy, resonance Raman spectroscopy and plasmon surface polariton enhanced Raman spectroscopy. (Hubbard 1995.) This research concentrates on the application of the basic Raman technique.

3.2.1 Raman Scattering

Along with absorption, the vibrations of a molecule can be also excited by a different mechanism, also referred to as Raman Effect. The Raman Effect is based on inelastic scattering of light quantum, which is caused by the interaction of monochromatic radiation and a molecule. The impact of monochromatic radiation on molecule leads to an exchange of vibrational energy according to equation 3. The energy of the scattering

light quantum can be higher or lower than the energy of the exciting radiation. This energy quantum formulates the Raman spectrum. (Schrader, Bougeard et al. 1995.)

$$hv_R = hv_0 \pm hv_s \quad (3)$$

where hv_R is the energy quantum [J]
hv_0 is the energy of the exciting radiation [J]
hv_s is the vibrational energy [J] (Schrader, Bougeard et al. 1995).

Together with the inelastic scattering, an elastic scattering phenomenon happens. This elastic scattering is referred to as Rayleigh scattering. Rayleigh scattering has, due to its elastic nature, an identical energy to the exciting radiation. (Schrader, Bougeard et al. 1995.)

The different nature of Raman and infrared spectroscopy enables them to be used as complementary techniques. As mentioned before, the polarization of a molecule enables vibrations to be detected in Raman spectrum. This polarization further enables the induction of a dipole moment in a molecule, when it enters an electric field. As the molecule enters an electric field, the electrons and nuclei residing in it are forced to move in opposite directions. The dipole moment is dependent on the electric field strength and molecular polarizability, as seen in equation 4. (Schrader, Bougeard et al. 1995.)

$$\left(\frac{\partial \alpha}{\partial q}\right)_0 \neq 0 \quad (4)$$

where α is the molecular polarizability [Cm^2/V]
q is the charge of the vibration [C] (Schrader, Bougeard et al. 1995).

3.2.2 Raman Spectrum

A Rayleigh scattering has a much greater chance of occurring when a light quantum collides with a molecule than Raman scattering. A visualization of Raman scattering is illustrated in figure 2. As seen in equation 3, there is a possibility for both a higher or lower quantum of energy to scatter from a molecule when it is radiated. The reason for this is the Boltsmann's law, which indicates that a small number of molecules reside in a vibrationally excited state in an ambient temperature. Because some of the molecules of the irradiated matter are already in excited state, a quantum of larger energy can be produced when the matter is radiated. (Schrader, Bougeard et al. 1995.)

In 1852, it was hypothesized that fluorescence and phosphorescence always produce light of a longer wavelength than that of the exciting radiation. This hypothesis was presented by Sir George Stokes, a prominent figure in the fields of fluid dynamics and physical optics at the time. Because of this, the lines seen in Raman spectrum are referred to as Stokes and anti-Stokes lines. Stokes lines are the lines that appear on the lower frequencies, i.e. higher wavelengths, than that of the exciting radiation, and anti-Stokes lines are the ones that appear on the higher frequencies, i.e. lower wavelengths. Stokes lines are created by the scattered energy that is of lower quantum than the irradiating light, and anti-Stokes lines are created by the scattered energy that is of higher quantum. Stokes lines are always more prominent than anti-Stokes lines. (Schrader, Bougeard et al. 1995.) These lines are visualized in figure 3.

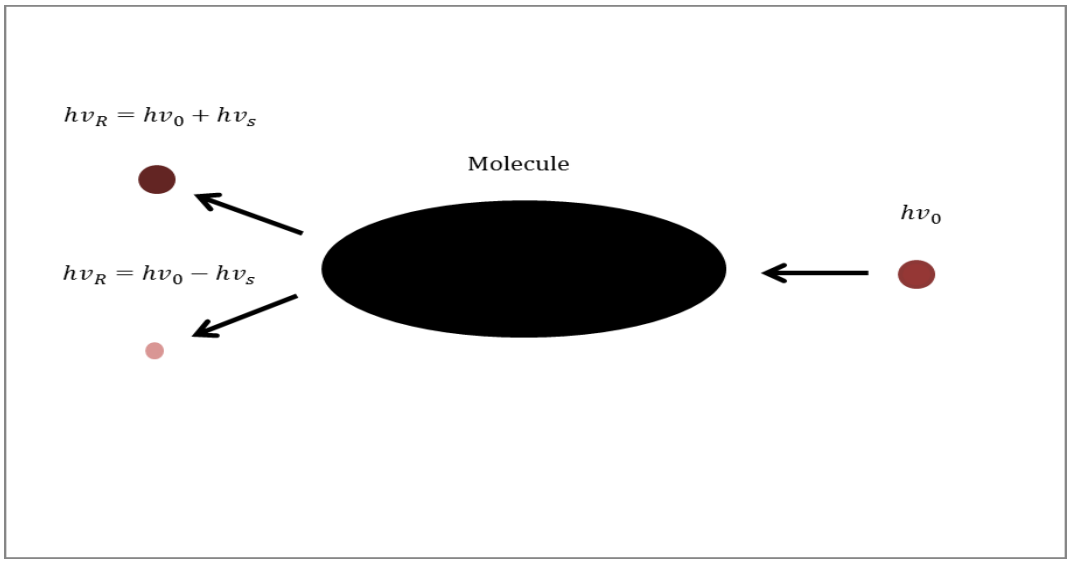

Figure 2. An illustration of Raman process, where radiation interacts with a molecule and scatters, either with lower or higher energy.

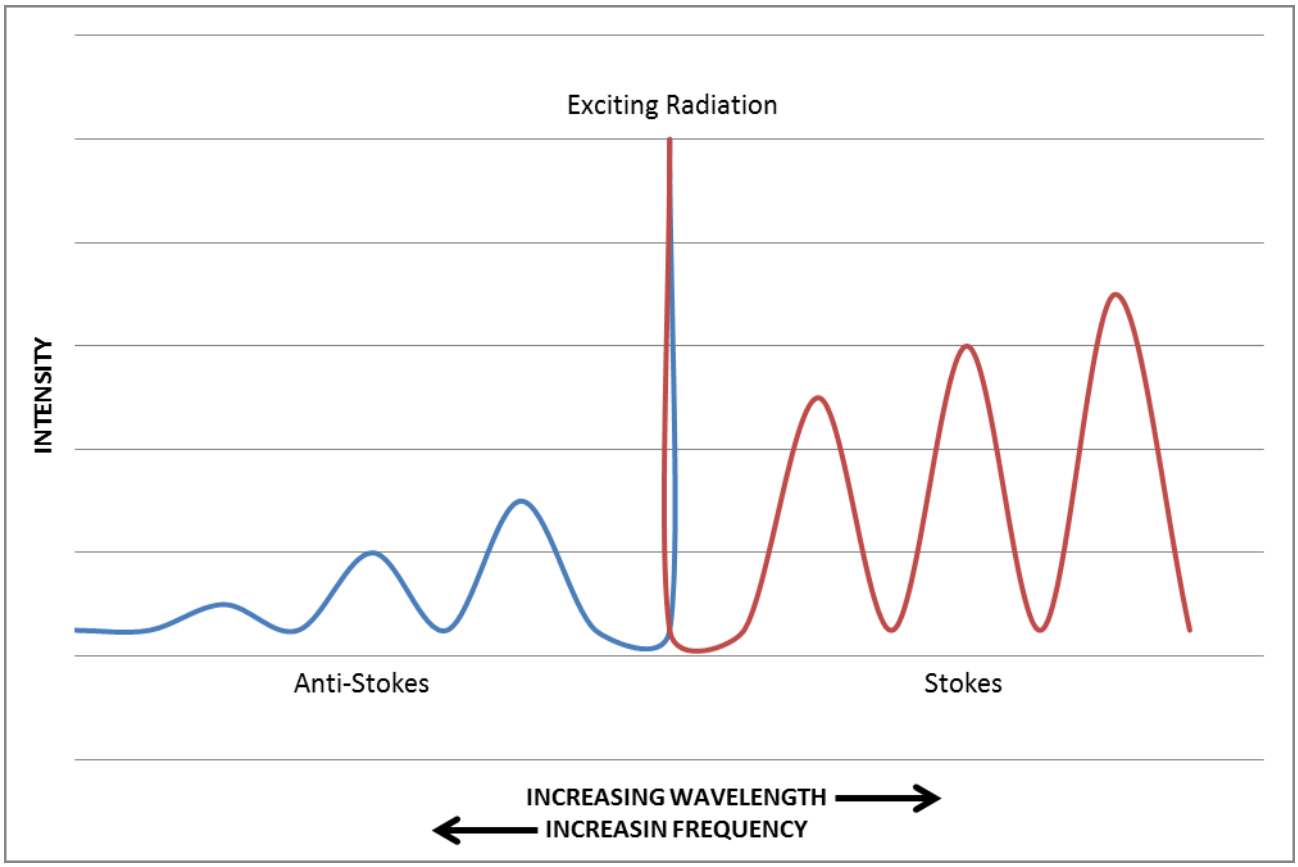

Figure 3. Anti-Stokes and Stokes lines in Raman spectrum in relation to the exciting radiation.

3.3 Spectral Properties of Minerals

Spectroscopy is a diagnostic tool that is sensitive to a wide variety of physical processes. This sensitivity can be seen as both positive and negative feature. The sensitivity of the technique leads to wide variety of applications, and is particularly useful for studying the structure and composition of minerals. On the other hand, the sensitivity can negatively affect the interpretability of resulting spectra due to susceptibility to slight changes in crystal structure and chemistry. (Clark 1995.)

The spectral properties of minerals have been widely studied over the years and the information gained has been used to explore the composition of the earth's surface. Due to the great diversity of minerals in our natural habitat, comprehensive analysis of minerals would be highly time consuming. Luckily, much of the mineral properties can be derived from four common structural elements, which are silicates, carbonates, sulfides, and hydroxides. (Eismann 2012.)

3.3.1 Effects of Crystal Structure and Chemistry

The sensitivity of reflectance spectroscopy makes it possible to differentiate endmembers from minerals of a given mineral series, as seen in figure 4. Reflectance spectroscopy is also able to differentiate prominent features of groups such as the hydroxyl group with more precision than for example the X-ray diffraction or XRD analysis, which is a popular method for determining crystallinity. This can be seen in figure 5 where the reflectance spectroscopy has the ability to clearly distinguish the mineral kaolinite from the mineral halloysite, whereas XRD analysis would classify both as the same mineral. (Clark 1995.)

In Raman spectroscopy, the intensity of the Raman scattered radiation can be enhanced by choosing the exciting frequency, i.e. the frequency of the radiation source, so that it is close to the absorption band of a studied crystal. When the exciting frequency is just below the frequency of the absorption band, the intensity of the scattered radiation is enhanced to the greatest degree, meaning that the features of the spectrum become the most prominent. (Loudon 1965.)

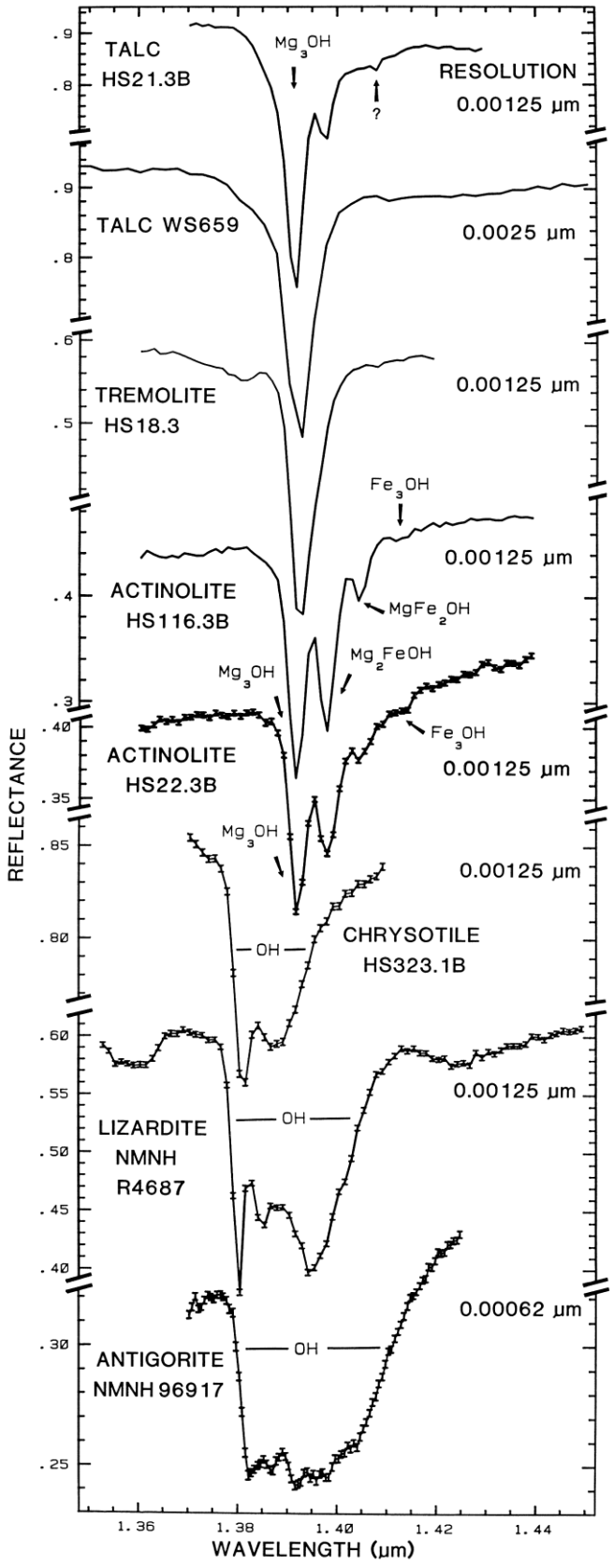

Figure 4. High resolution reflectance spectra of the first overtone of OH in selected minerals. It is worth noting that while the composition is constant, the absorptions change with small structural variations in chrysotile, lizardite and antigorite. (Clark 1995.)

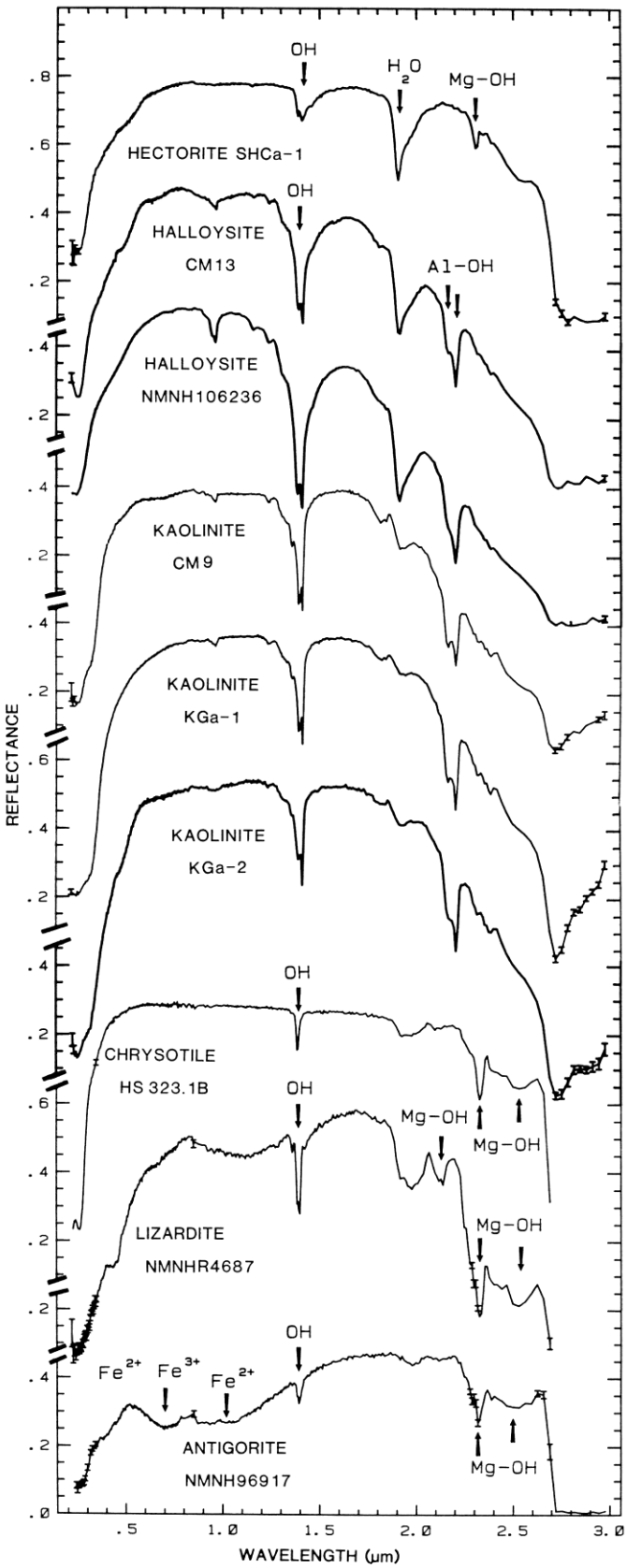

Figure 5. Reflectance spectra of selected minerals with indicated vibrational bands caused by OH. (Clark 1995.)

Scattering of photons makes reflectance spectroscopy possible. When photons enter a surface, they can be absorbed, or scattered from the surface allowing us to detect and capture these photons. The information recovered from reflectance spectroscopy is based on the wavelength dependency of the scattered and absorbed photons. (Van Der Meer 2004.)

If we take a look at Beer's law (see equation 1), we find that transmission represents an ideal case of scattering. This means that in transmission, when light passes through a material there is little to no scattering, whereas in reality some degree of scattering is always present. The analysis of reflectance represents a more practical application of Beer's law, where each time photons encounter a material grain, some of the photons are absorbed and some scattered. The ratio of absorbed and scattered photons depends on the brightness of the material grain. If the grain is bright (e.q. quartz), most photons scatter from the grain surface, whereas if the grain is dark (e.q. magnetite), majority of the photons will be absorbed at the grain surface. (Clark 1995.)

The intensity of reflectance in materials that are mixtures of dark and bright grains is greatly influenced by the darker grains. Even a relatively small percentage of dark grains in a material can severely reduce the overall intensity of spectra and in general, the darker components will always dominate the intensity in mixtures as seen in figure 6. (Clark 1995.)

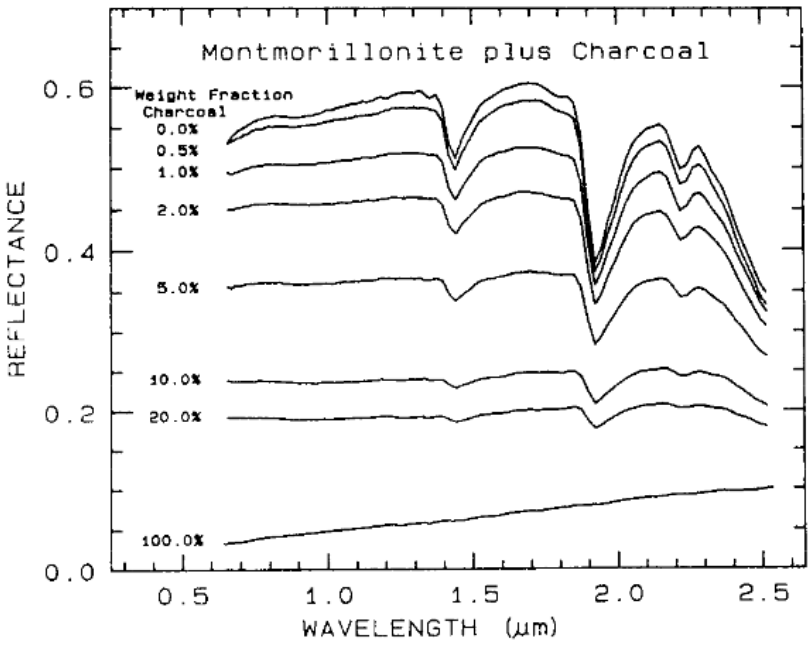

Figure 6. Reflectance spectra of montmorillonite and charcoal mixtures. The darkest substance, i.e. the substance with the most charcoal, dominates at a given wavelength. (Clark 1995.)

Grain size of a material greatly influences the ratio of absorption and scattering. Beer's law (see equation 1) indicates that a larger grain also has a larger internal path which contributes to the absorption of photons. This in turn means that in smaller grains, the proportion of surface reflections is greater than the proportion of internal photon path

length, i.e. the surface-to-volume ratio is greater in smaller grains than larger grains. The effect of larger grain sizes on reflectance is illustrated in figure 7. (Van Der Meer 2004.)

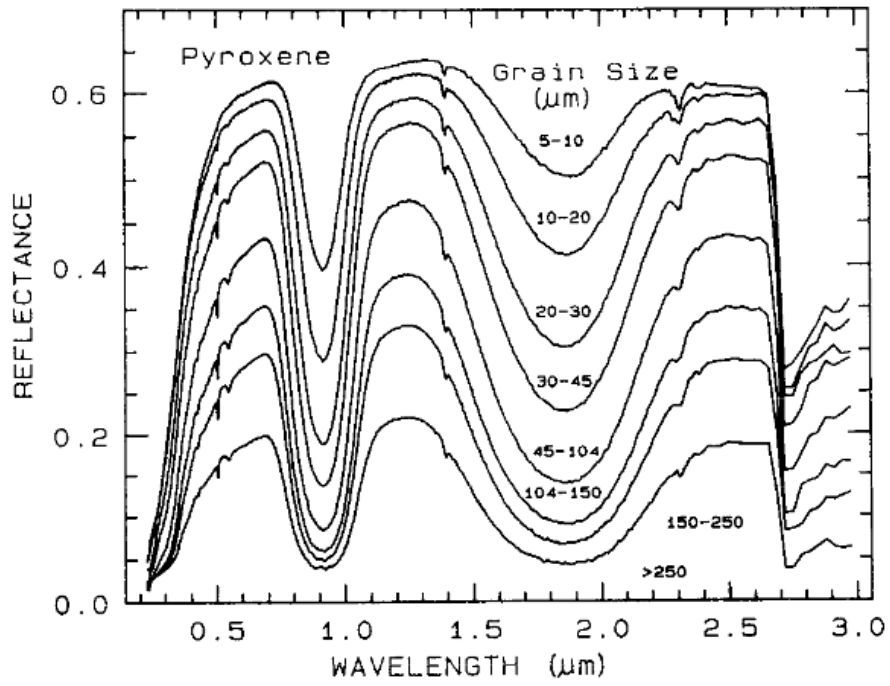

Figure 7. Reflectance spectra of pyroxene at different grain sizes. The larger the grain, the smaller the reflectance. (Clark 1995.)

Reflectance spectroscopy has an advantage of being a non-destructive method with no required sample preparation process. This leads to many possible applications for the technique, but the nature of the technique can also be restrictive. Reflectance spectroscopy does exhibit some insensitiveness in the visible and near-infrared regions. This is evident in the spectra of mineral quartz, which has no clear distinctive features in these regions. (Clark 1995.)

In Raman spectroscopy, the detection of finer grain sizes can be challenging. This is due to the surface scattering preventing the exciting radiation from penetrating deep into the crystal structure. This, in turn, leads to a situation where larger grain sizes dominate spectra in materials of mixed grain sizes. (Farmer 1998.)

4 Factors Affecting the Quality of the Aggregate

Aggregate material may consist of natural aggregate, manufactured aggregate or recycled aggregate. In this thesis we focus on the properties of the natural aggregate material. Natural aggregate refers to aggregate from mineral sources, which has been produced by using nothing more than mechanical processing. Both fine and coarse aggregate have their own standards of quality, which differ slightly from each other. Coarse aggregate generally refers to aggregate with particle sizes from 2 mm to 45 mm. Fine aggregate on the other hand refers to aggregate with particle sizes from 0.063 mm to 2 mm. (SFS-EN 13043.)

Aggregate has to fulfill distinct physical requirements for it to be qualified as a construction material. Fragmentation resistance, durability and resistance to wear by abrasion play a major role in these requirements. Aggregate is generally considered to be the most important material factor when analyzing the road wear caused by studded tires. The most significant aggregate characteristics include the abrasion resistance and the content of the coarse aggregates. The maximum size of the aggregate has, in some cases, a significant influence on the amount of wear, with larger size reducing wear. (Doré, Zubeck 2009.)

Fragmentation resistance and durability of aggregate can be determined with the Los Angeles test. The Los Angeles coefficient is calculated based on the test, and aggregate material is divided into classes based on these coefficients. The best class containing the hardest aggregate has a Los Angeles coefficient of 15 or below and the worst class containing the frailest aggregate has a Los Angeles coefficient of 50 or above. The resistance to wear can be determined by the Nordic abrasion test which Nordic abrasion value as a result. The aggregate material is divided into classes similarly as in Los Angeles test with the best class having values of 7 or below and the worst class having values of over 30. The hardness of the aggregate can also be estimated by tests measuring the resistance to polishing and by the micro-Deval test which measures the resistance to wear. (SFS-EN 13043.)

Mechanical crushing of aggregate can happen as a result of continuous traffic loading, material handling and physical or frost weathering. The frost weathering is especially common in Finland. The minerals of the fine aggregate formed by the mechanical crushing are referred to as residual material. The mineral composition of the fine aggregate that has been mechanically separated from the host aggregate doesn't differ significantly from that of the host aggregate. This means that the physical properties of the resulting fine aggregate can, to some degree, be estimated during the crushing of aggregate. The aggregate's resistance to mechanical wear depends on its hardness. This hardness is affected by the properties of the minerals forming the aggregate rocks and the way these minerals interlock. When considering the properties of the minerals, it is important to take note of their ability to resist scratching and fracturing. (Nurmikolu 2004.)

Some "soft" minerals in the mineral structure of the aggregate rocks can be beneficial for the overall firmness of the rocks. These "soft" minerals (e.g. micas) increase the elasticity of the rock structure and thus its ability to withstand stresses. The way the minerals are interlocked defines the scale at which the rock fractures along the grain surfaces. The rocks which have grains that are wedged together are generally firm because the wedged structure prevents clear fracture zones from forming. Fine grained

rocks are also generally firmer than coarse grained rocks. The fine grained rocks have more cohesion creating surface and rougher grain surfaces than coarse grained rocks. Whether the rock is foliated or not, also affects the firmness of the rock greatly. (Nurmikolu 2004.)

Environmental stresses affect the quality of aggregate considerably. The environmental stresses are caused mainly by the existence of water, temperature fluctuations and their combined effect. Frost weathering is the consequence of a frozen structural material. When the water freezes, it tries to expand its volume in the pores of material grains. This causes tension between the particles of the material. If this expansion is repeated over and over again, it can lead to weakening of particle structure and ultimately fracturing. The effect of the expansion of the in situ water is increased by water in the absorption and capillary pores. The water in these pores is able to stay in a liquid form even in freezing temperatures. The freezing of the gravitational water in the larger pores induces negative pressure to the whole pore structure, which in turn tries to pull the liquid water molecules on the surfaces of smaller pores towards the center of the freeze. The larger the amount of absorption pores, the more absorption water the rock can store. This means that the amount of water pulled towards the center of the freeze possibly increases and the pressure in the center of freeze becomes greater. (Nurmikolu 2004.)

The freeze weathering doesn't cause changes in the mineral structure of the aggregate; the wear inflicted on the rocks is purely mechanical. Aggregate weakened by the freeze weathering is susceptible to wear caused by traffic loading and supporting structures as well as chemical weathering due to the increased area of aggregate in contact with the environment. (Nurmikolu 2004.)

All chemical and physical weathering processes produce rock fragmentation. Chemical weathering also dissolves salts that may linger within the weathering profiles and drainage basins for lengthy periods of time. Some of these salts eventually precipitate thus preventing water infiltration in the area. (Riaza, Strobl et al. 2001.) Chemical weathering is a term used to describe the chemical reactions between the aggregate, atmosphere and water. The end products of these reactions are the residual materials of the rocks. These residual materials consist of products of weathering and solutions containing chemical elements from the rocks. This means that the chemical weathering alters the mineral structure of the rocks, as opposed to the mechanical wear caused by freeze weathering and traffic loading. (Nurmikolu 2004.)

Grain contacts in dry conditions enable mineral reactions to take place. When grain contacts happen in a moist space, more widespread effects are produced. Clays are produced when water reacts with feldspar, and acid weathering and soil conditions enable the formation of silica solutions during granitic weathering. The degree of weathering in a rock is also influenced by its degree of deformation and crystal stress. Rocks with more stress are more easily dissolved into solutions than unstressed ones. When chemical weathering happens on a granitic rock, the end-product is often gritty clay. Fragments and quartz crystals are the main cause of the grittiness. The clays produced by the reactions of feldspars and mica are typically multi-colored, brown or grey depending on the degree of iron oxidation. (Riaza, Strobl et al. 2001.)

All aggregates will undergo chemical weathering caused by the processes that are characteristic to them. Some of these processes include dissolution, oxidation and reduction. The chemical weathering is dependent on the chemical conditions of the environment.

As in freeze weathering, water is also a major factor in processes associated with chemical weathering. The extent of the chemical weathering depends on the amount of water available to dissolve the rock as well as the flow conditions determined by the porosity of the rock, density of the cracks and the position of the water surface. (Nurmikolu 2004.)

4.1 Factors of Mineral Firmness

Minerals can be divided into two groups based on their compression resistance. One of these groups is the stress (or negative) group. The other is the anti-stress (or positive) group, which consists of minerals that are more fragile and have less compact ion lattice. (GARDEMEISTER, KAURANNE et al. 1972.)

Usually, the minerals that crystallize first are able to assume their own structure. In granite, mica and feldspar crystallize first, and quartz, which is last to crystallize, will inhabit the spaces between the already crystallized mineral grains. When quartz is forced to crystallize in this manner, it will act as the "supporting structure" of the rock and thus strengthen the rock. Garnet is a typical example of a mineral that takes on a specific form when it crystallizes. The form of the crystals resembles berries with especially smooth surfaces. Although the garnet is a sturdy mineral, it can weaken the structure of a rock due to its weak bonding with neighboring minerals. In rapakivi granites, the shape of the feldspar closely resembles that of coarse round grained sediments. This greatly increases the granite's vulnerability to mechanical weathering. Rocks that contain lots of fibrous and splintery minerals, such as hornblende rich gabbro, have especially strong interlocked structure that can be likened to the arrangement of interlocking fingers. (GARDEMEISTER, KAURANNE et al. 1972.)

Every mineral has its own method of fracturing. The cracked fragments of some minerals resemble their crystal structure, as in for example galena. This is not always the case. Garnet, for example, almost always appears in specific berry-like crystal forms but fractures into blocks of indefinite shape due to the isotropic shape of its lattice. Likewise, quartz also has uneven and randomly oriented fracture surfaces. Some minerals, like feldspar, tend to fracture in specific pre-determined orientations. In these cases, one of the ion layers in the crystal lattice opens up more easily than others. (GARDEMEISTER, KAURANNE et al. 1972.)

Calcite fractures into rectangular blocks very easily in three nearly perpendicular directions. Feldspar has two distinct fracture orientations that form approximately a right angle with each other. The pyroxenes as well as amphiboles also have two fracture orientations. Mica have one distinct fracture orientation which enables them to be sliced into transparent slabs. These above mentioned differences in fracture orientation ensure that the compression resistance of minerals varies with the orientation. Minerals behave according to the elasticity theory only when the forces acting on the minerals are small in scale. If the scale of the forces is increased, in for example a triaxial test, the behavior of the mineral will first transform into plastic and then viscoelastic. This behavior is affected by the dislocation (i.e. the tendency to slip or snap) of the ionic crystals. They can move from one state another while keeping the crystals intact. (GARDEMEISTER, KAURANNE et al. 1972.)

4.2 Factors of Rock Firmness

Fine grained, compact and glass-like rocks are firmer than coarse or large grained rocks and the cohesion surface in fine grained rocks is significantly larger than in coarse or large grained rocks. This cohesion surface has greater strengthening effect than the quality of the microscopic grains of the rock minerals. It has been observed that the presence of water has a debilitating effect on the firmness of the rock. (GARDEMEISTER, KAURANNE et al. 1972.)

The velocity of a seismic wave through a rock is directly proportional to the density and degree of compactness of the rock. The porosity of sandstone and the velocity at which a wave moves through it correlate to the lateral pressure of the sandstone as shown in the figure 8. The same correlation has been observed between seismic velocity and compressive strength figure 9. These figures illustrate the effect compaction has on the strength of a rock, i.e. the more compact rock is generally stronger. (GARDEMEISTER, KAURANNE et al. 1972.)

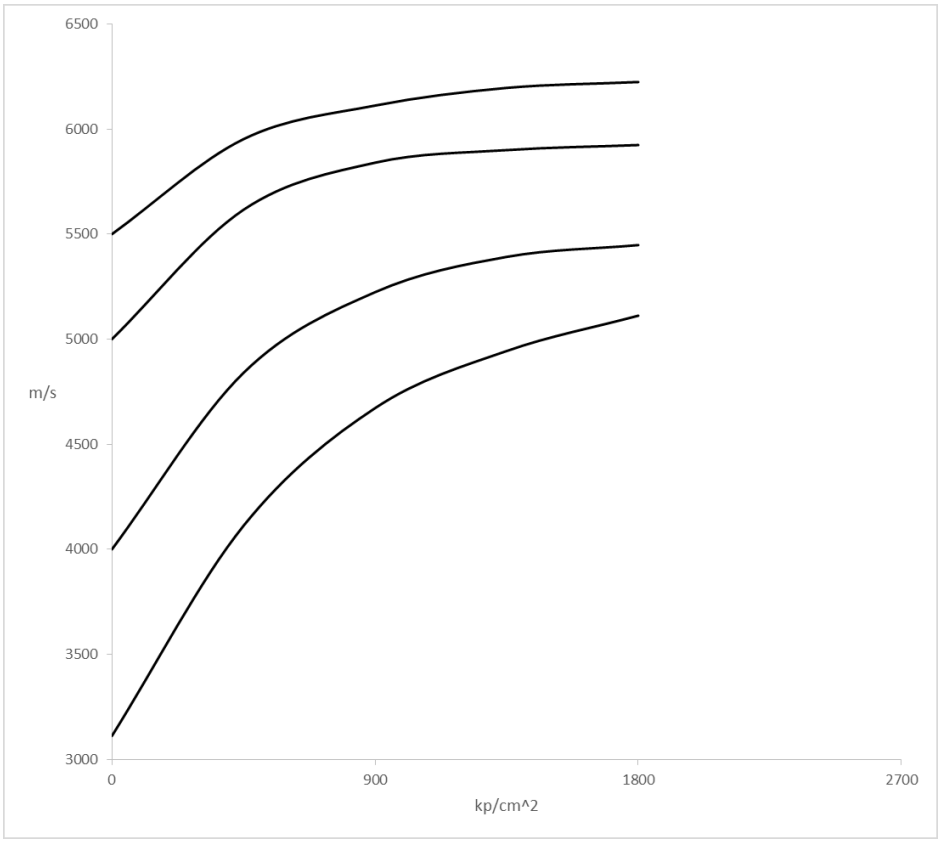

Figure 8. The dependency of porosity and the velocity of a seismic wave on lateral pressure in a sandstone. The two upper lines describe a sandstone with a porosity of 1.3 % with the two lower lines describing a porosity of 7.4 %. (Adapted from GARDEMESTER, KAURANNE et al. 1972.)

The effects of the mineral composition on the firmness of the rock are quite complex. This is due to the fact that all the minerals of a given rock have their own firmness, dislocation tendencies, shapes that affect the cohesion and friction of the rock. Different

minerals also tend to occur in different sizes in the rock structure. (de Vallejo, Luis I González, Ferrer 2011.)

Investigations on the rocks commonly used in pavement aggregates have given insight to their wear and impact resistance. It has been observed that feldspar and calcite reduce these resistances whereas hornblende, quartz, and the specific gravity increase the resistances. (GARDEMEISTER, KAURANNE et al. 1972.)

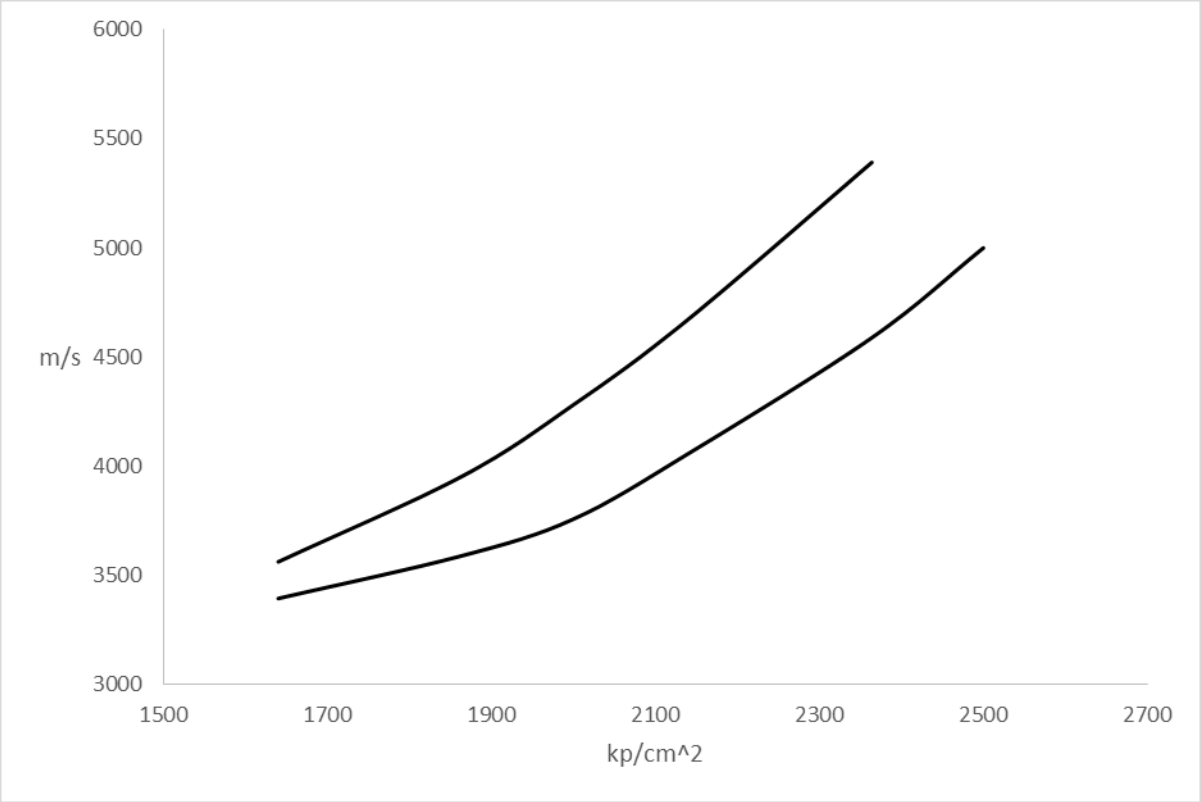

Figure 9. The relationship between seismic velocity and compressive strength. (Adapted from GARDEMEISTER, KAURANNE et al. 1972.)

A non-foliated, i.e. isotropic, rock is firmer than a foliated rock. This is due to the fact that in foliated rocks the weaknesses of the minerals are amplified when the minerals are located parallel to each other. An object has the smallest compression resistance when the stress is applied to it sideways against the flakiness. (de Vallejo, Luis I González, Ferrer 2011.)

Based on tests performed on different rocks, the compression resistance at its smallest is only half of the resistance measured when a rock is compressed perpendicular to the flakiness. Isotropic rocks also have a latent tendency to fracture in given directions that are usually perpendicular to each other. This tendency is caused by the internal stresses of the rock. (GARDEMEISTER, KAURANNE et al. 1972.)

A homogenous, isotropic soft or weathered rock will shear at an angle of about 45 degrees from the compressing force (e.g. shale). The shear of a schistose rock depends on the angle between the schistosity and the compressing force as shown in the figure 10. The foliation of a rock affects not only its firmness but also the size of the deformation as seen in figure 11. When the variation of the compressive resistance is about 50 % of

the foliation, the variation of the deformation can be as much as 150 %. (GARDE-MEISTER, KAURANNE et al. 1972.)

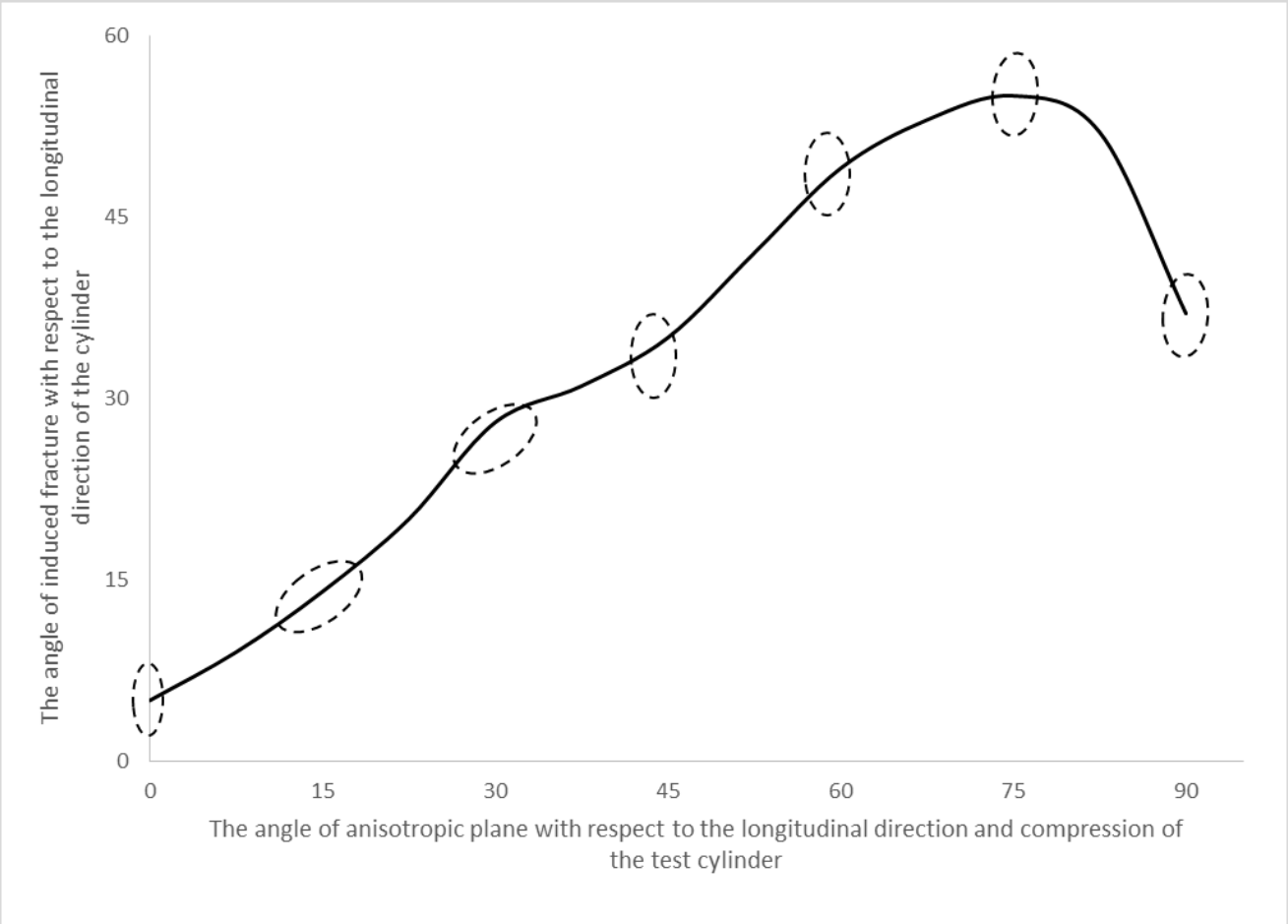

Figure 10. Shear of a schistose object. (Adapted from GARDEMEISTER, KAURANNE et al. 1972).

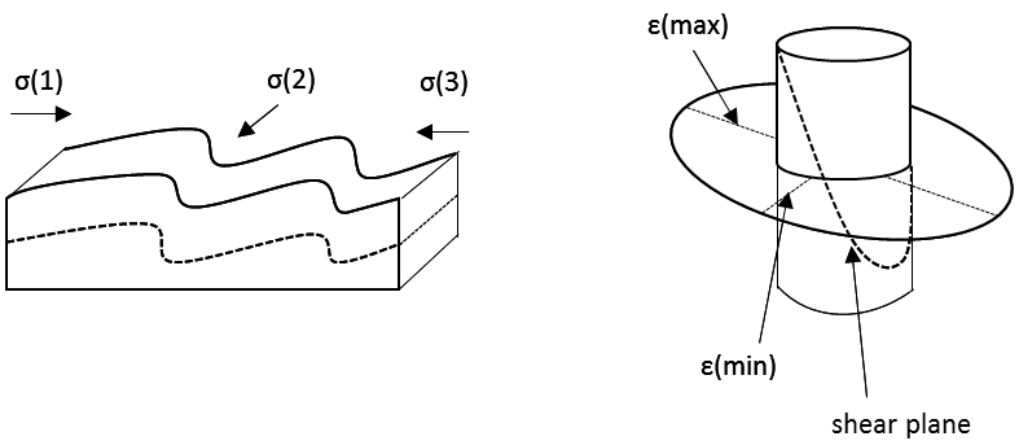

Figure 11. The effects of foliation on the shear strength of a rock (left picture, σ(3) > σ(1) > σ(2)) and on the deformation of a rock (right picture). (Adapted from GARDEMEISTER, KAURANNE et al. 1972).

5 Aggregate Classification Based on the Mechanical and Physical Properties

Different standards have been created to classify aggregates based on their mechanical and physical properties. The most important of these standards are SFS-EN 1097-9 and SFS-EN 1097-2, which describe the execution of the Nordic abrasion test and the Los Angeles test respectively. The Nordic abrasion test focuses on the examination of the resistance to wear by abrasion whereas the Los Angeles test focuses on the fragmentation resistance of the aggregate.

Aggregates can be classified based on the Nordic abrasion value and the Los Angeles coefficient obtained through their respective tests. The lower the coefficient values, the higher the durability of the aggregate.

The aggregate is classified as high-grade if its Los Angeles coefficient is below 20 and its Nordic abrasion value is below 10. High-grade aggregate can be used on high volume tarmac roads, highway pavements and structural layers of railway corridors. The aggregate is classified as medium-grade if its Los Angeles coefficient is above 20 but below or equal to 30 and its Nordic abrasion value is above 10 but below or equal to 19. Medium-grade aggregate can be used on lower volume tarmac roads, structural layers of highway corridors, surfacing and structural layers of gravel roads, structural layers of railway corridors and in general construction. If the aggregate has a Los Angeles coefficient of above 30 and a Nordic abrasion value of above 19, it is classified as low-grade. Low-grade aggregate can be used in general construction without clear quality specifications as well as on surfacing of gravel roads and on subbase of highway corridors. (Geological Survey of Finland, GTK.)

5.1 Nordic Abrasion Test

The Nordic test is used to determine the resistance to wear by abrasion from studded tires in coarse aggregates. The test can be applied to aggregates with a size fraction between 11,2 mm and 16 mm. The test is conducted with a waterproof follow drum that has been sealed from the other end. The inside diameter of the drum is (206,5 ± 2,0) mm and the internal length of the drum is (335 ± 1) mm. The minimum wall thickness of the drum is 6,0 mm. The drum must be closed by a flat lid that is fitted with watertight and dust seals and is at least 8 mm thick. (SFS-EN 1097-9.)

Three ribs, each with a length of (333 ± 1) mm, are mounted on the interior of the drum to improve the mixing of the aggregate particles and the steel balls. These ribs are mounted with an equal spacing. The ribs must be preground for (24 ± 1) hours before first use. (SFS-EN 1097-9.)

The mass of the intended laboratory sample must be large enough to prepare four test specimens. The grading of each of the test specimens must have (65 ± 1) % of the particles passing the 14,0 mm sieve, meaning that (35 ± 1) % of the test specimen must consist of particles in the size range of 14,0 to 16,0 mm. Each test specimen must have an initial dry mass defined according to the following formula:

$$M_1 = \frac{1000\rho_p}{2{,}65} \pm 5 \quad (5)$$

where M_1 indicates the initial dry mass of the test specimen [g]
ρ_p indicates the particle density determined according to EN 1097-6:2013 [Mg/m^3] (SFS-EN 1097-9.)

The laboratory sample is washed on the 2 mm sieve and dried to constants mass in the oven at (110 ± 5) °C. After drying the sample is cooled to ambient temperature. Once the sample has reached the ambient temperature, it is sieved according to EN 933-1 to provide a sufficient amount of material for the preparation of at least two test specimens. The 11,2 mm, 14,0 mm and 16,0 mm sieves are used in the preparation to give two separate particle size fractions of 11,2/14 mm and 14/16 mm. The size fractions are reduced in accordance with EN 932-2:1999, Clause 11, if needed, to achieve a test specimen of the specified composition. (SFS-EN 1097-9.)

The test is carried out by first placing the abrasive charge into the drum. The abrasive charge consists of steel balls with the diameter of (15,0 + 0,1/-0,5) mm and a total mass of (7000 ± 10) g. After the abrasive charge is placed into the drum, the test specimen is added. Finally (2,00 ± 0,01) l of water is also added. (SFS-EN 1097-9.)

The drum is rotated with electrical motor at a regular speed of (90 ± 3) r/min for (5400 ± 10) revolutions. After the rotation, the aggregate and the steel balls are collected separately taking care not to lose any aggregate particles. The retained aggregate particles are placed onto a tray. The tray and its contents are dried to constant mass in the oven at (110 ± 5) °C. After drying the mass of aggregate particles greater than 2 mm is determined by dry sieving according to EN 933-1. The mass, M_2, is recorded to the nearest gram. The procedure is repeated on a second test specimen. (SFS-EN 1097-9.)

The Nordic abrasion value is calculated for each test specimen with the following formula:

$$A_N = 100(M_1 - M_2)/M_1 \quad (6)$$

where A_N indicates the Nordic abrasion value [-]
M_1 indicates the initial dry mass of the test specimen [g]
M_2 indicates the dry mass of aggregate particles greater than 2 mm after abrasion [g] (SFS-EN 1097-9.)

The mean of the two values is calculated. The mean value is recorded if the difference between the values for the two test specimens is smaller than or equal to 10 % of the mean value. If the difference is greater than 10 % of the mean value, two further test specimens are tested. Further testing can be omitted if the results of the first two test specimens are below 5.0. If further tests are required, the standard deviation of the four A_N values must be calculated. In the case that the standard deviation is greater than 9 % of the mean of the four values, any suspect extreme values must be examined and discarded if needed according to the following procedure. (SFS-EN 1097-9.)

The four results, A_{N1}, A_{N2}, A_{N3} and A_{N4}, are arranged in order of magnitude. The following two quotients Q_1 and Q_2 are calculated:

$$Q_1 = (A_{N2} - A_{N1})/(A_{N4} - A_{N1}) \quad (7)$$
$$Q_2 = (A_{N4} - A_{N3})/(A_{N4} - A_{N1}) \quad (8)$$

If the value of either of these quotients is above 0,829, the suspected extreme value is discarded. After all the necessary extreme values are discarded, the mean of all accepted values is calculated. The mean value of the accepted values is reported to the nearest single decimal place. (SFS-EN 1097-9.)

5.2 Los Angeles Test

The Los Angeles test is used for determining the fragmentation resistance and durability of coarse aggregates. The result of the Los Angeles test is the Los Angeles coefficient or LA. The Los Angeles coefficient is obtained by rolling a sample of aggregate with steel balls in a specified Los Angeles testing drum. The aim of the rolling is to determine the quantity of crushed material retained on a 1,6 mm sieve. After rolling the weight percentage of the retained material is calculated from the original sample. (SFS EN 1097-2.) After the Los Angeles coefficient is calculated, the material can be analyzed. The higher the coefficient, the lower the fragmentation resistance of the material.

At the beginning of the test the sample is dried. After the sample has dried, it is sieved using 10 mm, 11,2 mm (or 12,5 mm) and 14 mm test sieves to achieve separate fractions in the ranges of 10 mm to 11,2 mm (or 12,5 mm) and 11,2 mm (or 12,5 mm) to 14 mm. Each of these fractions is washed separately and dried to constant mass. The fractions are allowed to cool to ambient temperature before mixing the two fractions to provide a modified laboratory sample comprised of aggregate passing the 14 mm test sieve but not the 10 mm test sieve. Additionally the grading of the test portion has to comply with at least one of the following requirements:

a) 60 % to 70 % passes a 12,5 mm test sieve; or
b) 30 % to 40 % passes a 11,2 mm test sieve. (SFS EN 1097-2.)

The test portion is placed carefully in the Los Angeles testing drum containing 11 steel balls. The drum is rotated for 500 revolutions at a constant speed. After the revolutions have ended, the aggregate is poured into a tray placed under the apparatus. The material from the tray is analyzed by washing and sieving using a 1.6 mm sieve. The portion retained on the 1.6 mm sieve is dried at a temperature of 110 °C until a constant mass is achieved. The Los Angeles coefficient is calculated from the following equation:

$$LA = \frac{5000 - m}{50} \quad (9)$$

where m indicates the mass retained on the 1,6 mm sieve [g]
5000 indicates the mass of the sample [g] (SFS EN 1097-2.)

6 Methodology

Spectral methods were used to classify rock samples based on their mineral content. These rock samples were collected from Seepsula quarry located in southern Finland. A total of 91 rock samples were included in these measurements. These samples consisted of 34 low-grade rocks and 57 sturdier, medium grade rocks. These grades were based on both, a visual assessment by a geologist, and results of a Los Angeles test. The area of Seepsula quarry belongs to a granitoid complex formed in early Proterozoic era (Lehtinen, Nurmi et al. 1998b).

The Los Angeles test is used to test mechanical hardness of rocks. The rock type of the low-grade sample was determined to be pegmatitic granite and the medium grade sample was determined to be quartz-feldspar gneiss. Fragmentation resistance and durability of these rock samples was determined using Los Angeles test and the obtained coefficients were 22 for the medium grade rock and 34 for the low-grade rock indicating a clear difference in the hardness's of the rocks.

In addition to the quarry samples, reference samples were measured from the endmember minerals of the rock samples. The sample rocks were determined to consist mainly of five endmember minerals; potassium feldspar or K-feldspar, quartz, anorthite, almandine and iron rich biotite.

6.1 Data Acquisition

The data for this research was gathered using two complementary spectroscopy techniques, reflectance spectroscopy and Raman spectroscopy. As explained in previous chapters, these two techniques complement each other due to the different molecular transitions they are able to detect during vibration, i.e. for a transition to be Raman active a change in polarizability must occur in the molecule, and for a transition to be infrared active a dipole moment change in the molecule must occur.

Data acquisition process also differed between the methods, mostly due to the different achievable resolutions. The data acquisition principles for each technique, and the setups used, are discussed in more detail in the following sections.

6.1.1 Reflectance Spectroscopy

Reflectance measurements included in this thesis were done using a combination setup of two different spectrometers. One of these spectrometers was able to detect the visible range of the electromagnetic spectrum, whereas the other was able to detect the near infra-red range. The samples used for the measurements consisted of 34 low-grade and 57 medium-grade rocks harvested from Seepsula quarry in southern Finland.

The setup used for the measurements is illustrated in the figure 12. As mentioned previously, two different spectrometers were used to detect the spectrum of the light reflected from the sample. The NIR (or near-infrared) range of electromagnetic spectrum was detected using Ocean Optics NIRQuest512 spectrometer, with a covering range of 900 – 2500 nm. The visible range of electromagnetic spectrum was detected using Ocean Op-

tics HR4000CG-UV-NIR high resolution spectrometer, which was able to cover the ranges of 190 – 1100 nm. As we can see, these spectrometers overlap each other in the range of 900 – 1100 nm. This problem was solved in the data analysis by only covering the range of 190 – 900 with the visible range spectrometer in the final analysis. A halogen lamp was used as a light source to excite the sample, and the power output was adjusted using an AXIOMET AX-3005DS power supply. The reflectance spectra were captured using a reflection probe in conjunction with a lens and an iris for efficient background noise removal. Bifurcated optical fiber was used to direct the reflected light to the spectrometers. The bifurcated optical fiber consisted of two optical fibers, one of them being a high OH fiber and the other being low OH fiber. High OH fiber can carry ranges of 250 – 1200 nm, while the low OH fiber can carry ranges of 400 – 2400 nm. This ultimately limited the spectral range of the setup to 250 – 2400 nm. The high OH fiber was connected to the visible range spectrometer and low OH fiber to the NIR range spectrometer. A fixed distance of 5 cm was used between the sample and the reflection probe to optimize the measurements and to prevent unnecessary data variance.

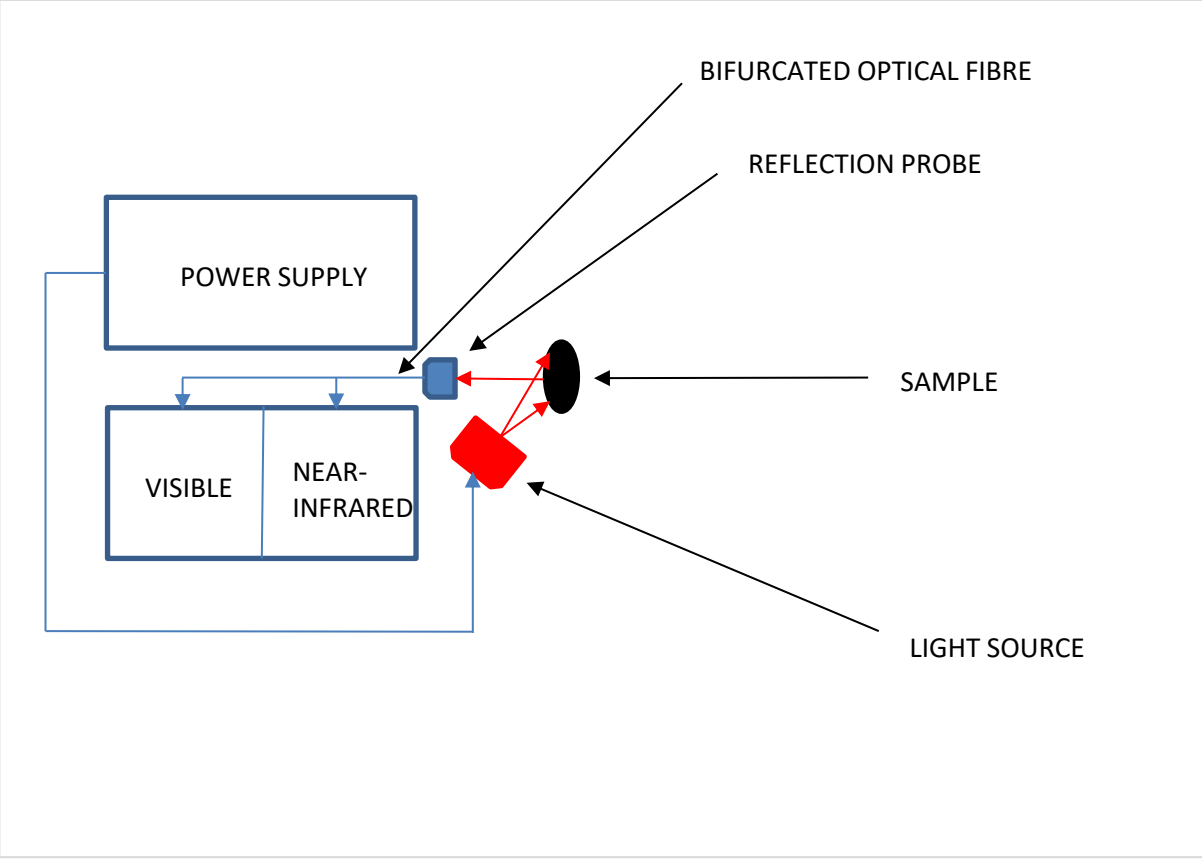

Figure 12. The setup used for the reflectance measurements. The visible and near-infrared indicate the two spectrometers used in the setup.

The measurements were conducted by first removing the background noise from the instrument. After the noise was removed, the instrument was calibrated by taking a reference measurement from a spectralon panel, which acted as a reflectance of 99 percent. These calibrations were done separately after each of the samples. During the measurements it was observed that the removal of the background noise after each of the samples is essential to eliminate potential distortions in the near infra-red region. These distortions greatly affected the shape of the reflectance spectra. The reflectance spectra

were always measured from the coarse surface of the rock sample. This was done to ensure that the resulting spectra would represent the natural state of the rock. The same distance was always kept between the measured sample and the spectrometer to minimize the possible distortion caused by the angle of the light emitted by the light source of the setup.

6.1.2 Raman Spectroscopy

The Raman spectroscopy measurements were conducted by first choosing the most representative samples of each rock sample class, i.e. low-grade and medium-grade. After the samples were chosen, the irregular rock samples were shaped into rectangular finer samples. One of the faces of each rectangle was polished to minimize angular differences in the rock surface and to ensure a more exact measurement. The measurement area was separated using non-reflective tape to avoid irregularities in the spectra.

The setup used for the measurement is illustrated in the figure 13. Andor Shamrock 750 spectrograph was used to capture the scattered light and direct it to Andor iStar 734 high-resolution camera with 18 mm diameter intensifier, which was used to record the spectrum of the Raman scattering. The wavelength of the laser source used in the setup was 532 nm. The optics used in the setup are illustrated in the figure 13. Band pass filter was used to eliminate all the other wavelengths than 532 ± 2 nm from the light emitted by the laser source. Long band pass, on the other hand, was used to prevent the scattered laser light (Rayleigh scattering) from entering the spectrograph when the sample was excited, i.e. the long band pass allows only the Raman-shifted signal light to pass through to the spectrograph from the sample. The setup was first calibrated using a pure calcite sample. The calibration was done to eliminate possible wavelength displacement from the spectrum.

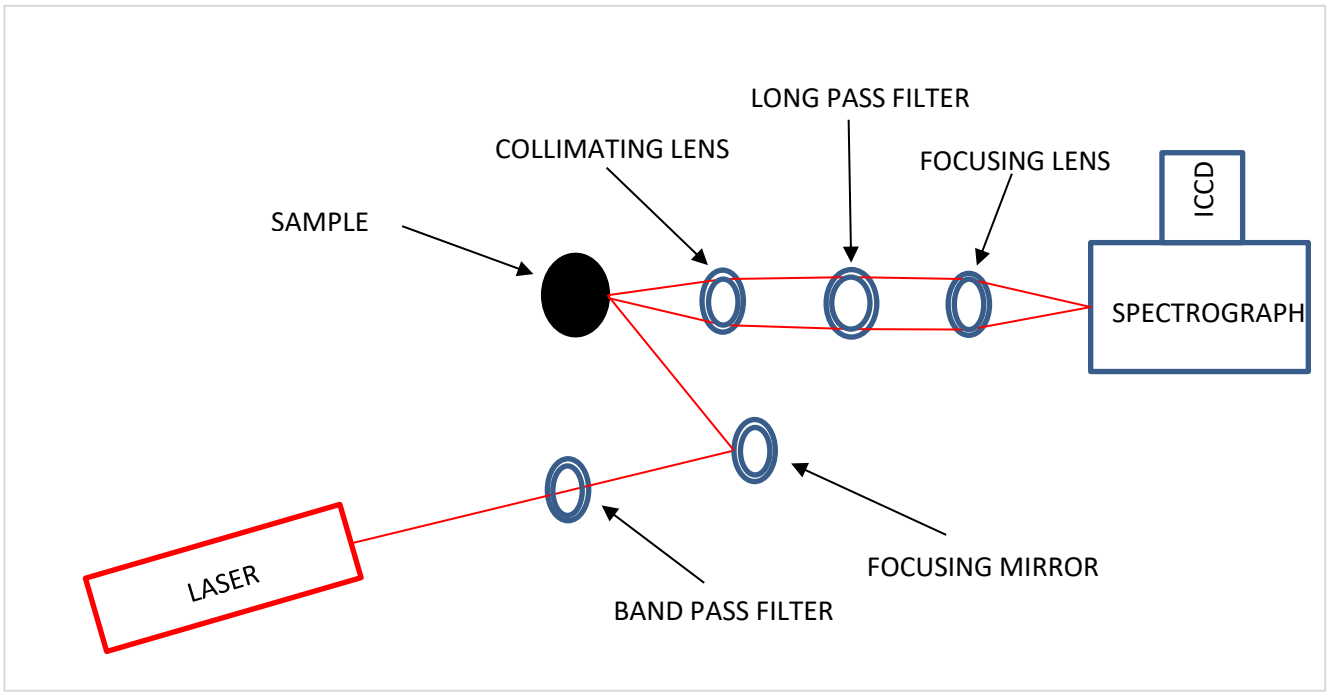

Figure 13. The setup used for the Raman spectroscopy measurements. ICCD refers to the intensified CCD camera used in the setup. CCD refers to the specific sensor used in the camera.

Measurements were conducted on the polished face of the rectangle. The measurement points were aligned so that the first measurement point was always at the bottom left-hand corner of the sample. Consequent points were measured by shifting to the right in 35 steps with a width of 0.5 mm. This completed the first measurement line consisting of 35 data points. After the first line was measured, the laser was moved upwards by 1 mm. The second data line was then measured from right to left using the same 35 steps. This process was continued so that ultimately 10 lines of 35 data points, i.e. 350 data points in total, was achieved per sample. The low-grade rock sample was chosen to be measured first, because the different minerals were visually easier to recognize, partly due to the larger grain size.

6.2 Data Pre-Processing

All the collected raw data needed to be pre-processed before any distinct analyses could be made. Data pre-processing is an important step in the data analysis because it can be used to increase the quality of the sample data significantly. The pre-processing methods used for the data were continuum removal, data smoothing and data normalization. These methods are described in more detail in the following paragraphs.

6.2.1 Continuum Removal

Continuum removal is used to standardize the raw data. Raw spectral data often exhibits a continuum that gives it a certain pronounced shape as shown in the figure 14. This continuum often complicates the data analysis because it can hide certain features in the spectrum. By removing the continuum from the data, the individual features of different spectra can be analyzed more clearly and compared more easily. Continuum removal is performed by first fitting a polynomial to the data. The data is then normalized to this polynomial. The results of the continuum removal to the appearance of the spectrum are shown in the figure 15.

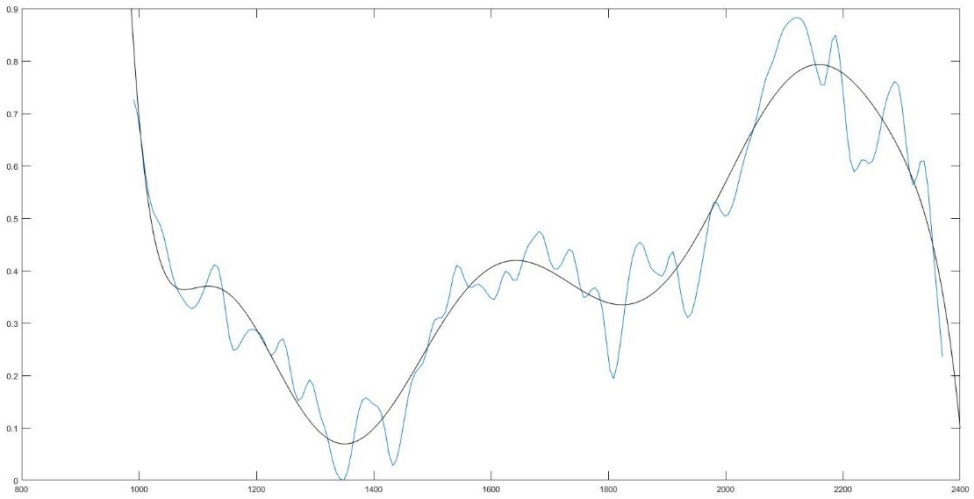

Figure 14. Raw spectral data with a pronounced continuum effect.

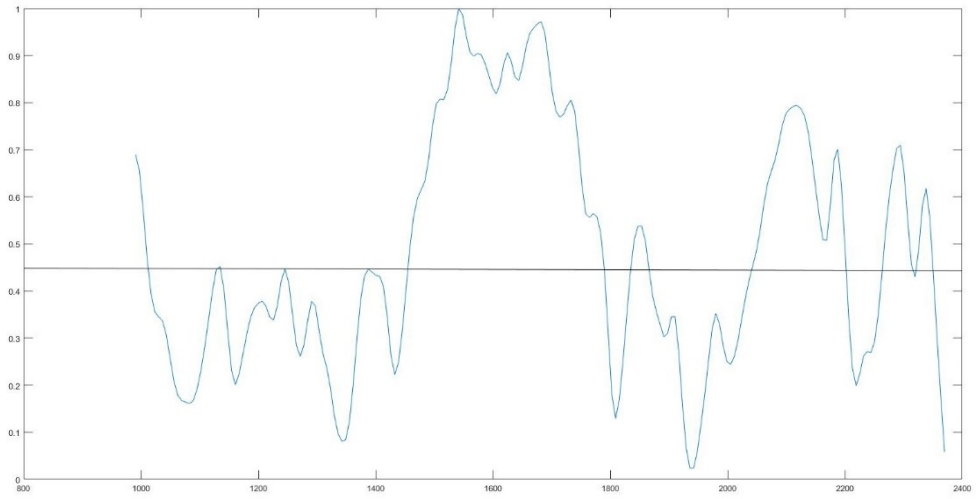

Figure 15. Raw spectral data, where the continuum effect has been removed.

6.2.2 Data Smoothing

In the case of the reflectance measurements, the data had to be smoothed to prevent distortion caused by the two separate spectrometers and eliminate dead pixels in the measurement configuration. Smoothing techniques are primarily used to obtain a de-noised set of a given raw spectra (Randolph 2006). Data smoothing was applied to capture the important patterns in the data, while at the same time eliminating unnecessary noise. The smoothing process was not performed to the Raman spectrometer data, mainly because of the high quality of the data. The effect of smoothing on the raw data is illustrated in figure 16 and figure 17.

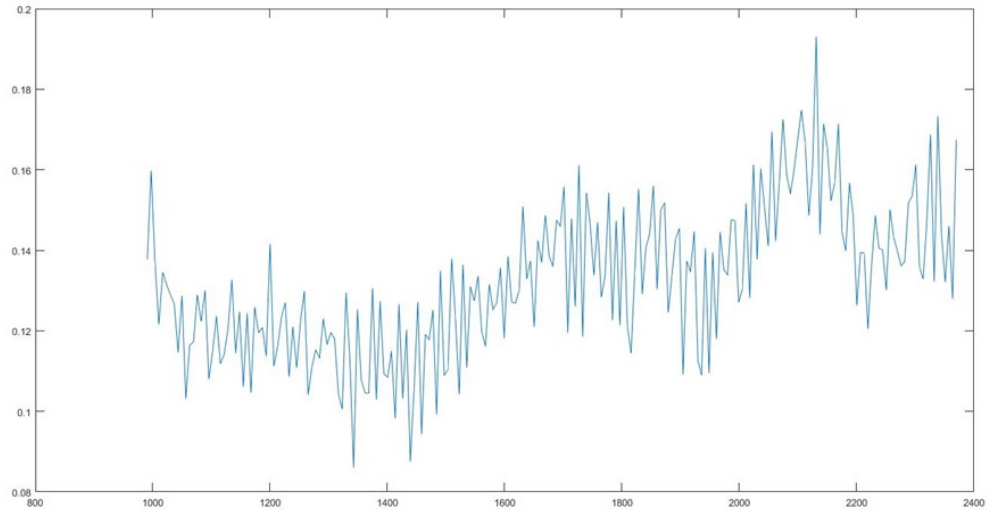

Figure 16. Raw spectral data with considerable noise.

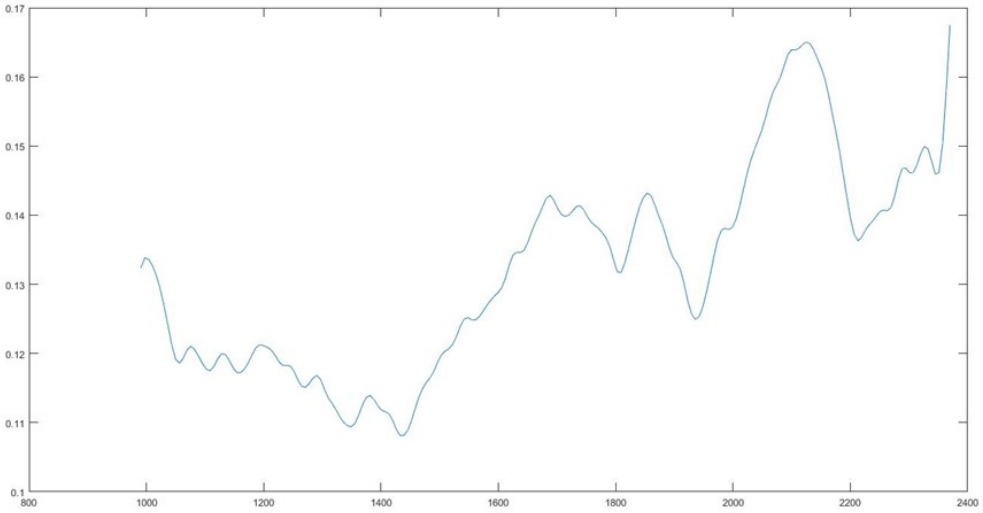

Figure 17. Smoothing performed on the raw data, features can be clearly observed.

6.2.3 Data Normalization

Data normalization is applied to the raw data to allow for more effective comparison between samples that are often heterogeneous. The goal of the normalization process is to numerically eliminate the constitutional differences in the collected data samples (Randolph 2006). In this thesis, a popular spectral approach was used where data is normalized in regards to its intensity (or reflectance value). The raw data was normalized between values of 0 and 1 to standardize data samples of different intensity or reflectance scale. The difference between non-normalized and normalized data is shown in figures 18 and 19.

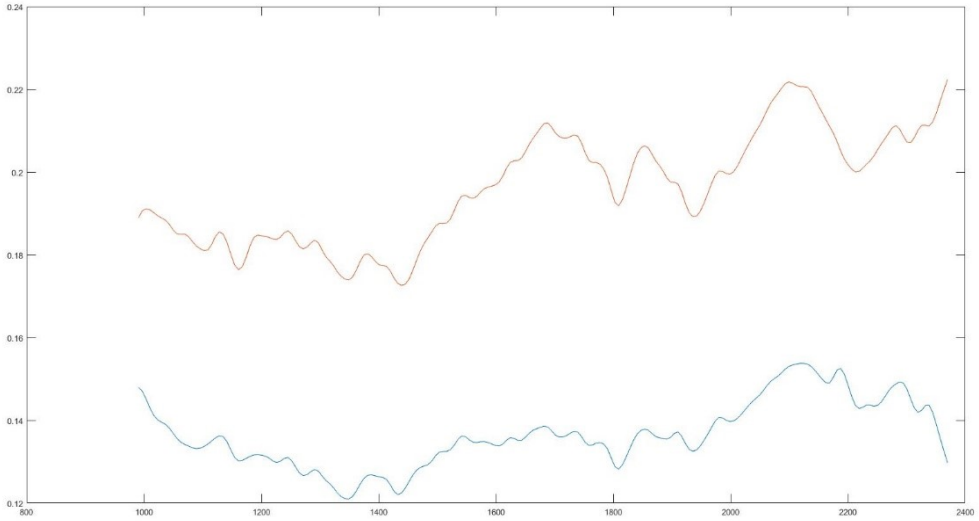

Figure 18. Spectral data with no normalization between them.

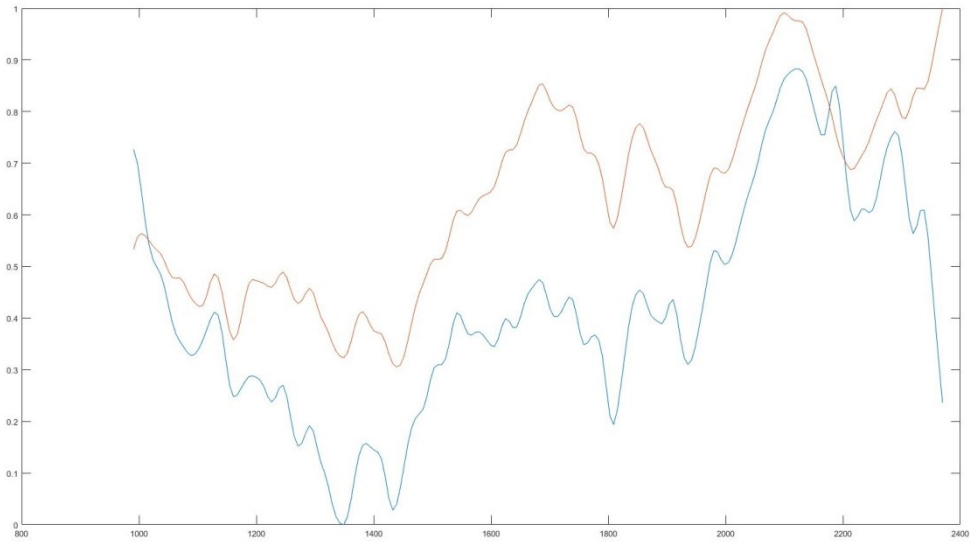

Figure 19. Normalized spectral data.

6.3 Data Processing

The data processing and analysis was performed using both physically based classification methods and statistical classification methods. Machine learning was implemented as a part of the statistical classification. The classification methods were chosen based on their suitability for classifying data in two distinct classes. Because of the low number of different classes, the classification performed was essentially binary classification. The principal idea for all the classification methods was to investigate how well they could differentiate between data that was gathered from two rock types of different hardness grade.

In both physically-based methods, the individual data was compared to the mean data of a given class using different classification methods. Statistical classification methods consisted of supervised and unsupervised learning methods as well as a linear correlation method, Pearson correlation coefficient. Machine learning was used to first train a classifier using a given data. This classifier was then used on new data (or probabilistic observations) and the accuracy of classifier was determined when classifying new data.

The aim of the statistical classification was to provide an alternative method for physically-based classification and to explore different analyzing techniques for optimal classification accuracy. The statistical methods differ fundamentally from physically-based methods. In physically-based classification, the classification decision is made based on the similarity of physical attributes within a space, whereas statistical classification aims to use different statistical algorithms to first study the attributes of a given data set and generate a model based on these attributes. This model then generates predictions on a completely new data set. In essence, statistical classification is based on algorithms that make the decision whether to classify a data sample to a given class.

Pearson correlation coefficient was implemented to assess the general linear correlation between the mean spectrum of a given class and the samples in that class. It was hypothesized that a sample of the given class would have relatively high positive correla-

tion values with the mean data of the same class, and relatively high negative correlation values with the mean of the opposite class.

The overall goal was to discover a classification method that would be reliable in classification of both medium-grade and lower-grade rocks when new data was introduced. Physically-based classification methods were applied to both infrared and Raman spectroscopy data. Instrument specific classification methods will be discussed in section 7.3.2 and 7.3.3.

6.3.1 Physically-Based Classification Methods

Physically based classification methods comprised Spectral Angle Mapper, which measures the spectral angle between given spectra, and Euclidean distance, which measures the spatial distance between given spectra. Physically-based methods are ideal for examining the similarity between two spectra and generally, the smaller the angle or the distance between the spectra, the more similar the spectra are with zero value meaning complete similarity between spectra. In general, physically based classification methods, SAM in particular, are less sensitive to disturbance caused by different lighting conditions, e.g. shady areas over an observed scene. However, physically-based methods tend to be sensitive to any excessive noise in the spectra. This problem was remedied by smoothing the raw data as explained section 7.3.2.

In infrared data classification, physically-based methods were used to compare individual data spectra to the mean spectrum of a given class, medium-grade or low-grade. It was hypothesized that the spectral angle (Spectral Angle Mapper) and the spectral distance (Euclidean distance) would both be smaller when the individual data was compared to the mean of assumed data class, and higher when compared to the mean of the opposite class.

In Raman data classification, physically-based methods were used to compare the individual data spectra to reference spectra of known minerals. Individual spectra were compared to four different mineral spectra, and classified to the mineral group with which the individual spectra had the smallest spectral angle or spectral distance. In Raman data classification, only the most representative sample from both classes was analyzed, whereas in infrared classification all the samples were analyzed as whole. This decision was made due to the instrumentation, as mentioned in section 7.2.

The Spectral Angle Mapper or SAM is a formulation that attempts to acquire the specific angles between a given image or data spectrum and the reference spectrum by depicting them as vectors in a space. The dimensionality of this space is equal to the number of bands in the used measuring instrument. The basic equation behind the SAM principle can be formulated as follows:

$$\alpha = \cos^{-1} \frac{\sum XY}{\sqrt{\sum(X)^2 \sum(Y)^2}} \quad (10)$$

where α is the angle formed between reference spectrum and image spectrum [°]
X is the image spectrum [-]
Y is the reference spectrum [-]. (De Carvalho, Meneses 2000.)

The value retrieved from the equation is expressed in radians, and the angle α shows the major similarity among the investigated spectra. The angle may obtain variation values between 0° and 90°. The aforementioned equation can also be formulated with cos α, in which case the best values that can be obtained are close to 1. (De Carvalho, Meneses 2000.) The equation is formulated as follows:

$$\cos\alpha = \frac{\sum XY}{\sqrt{\sum(X)^2 \sum(Y)^2}} \quad (11)$$

The Euclidean metric or Euclidean distance, d_E is defined by the following equation:

$$\|x - y\|_2 = \sqrt{(x_1 - y_1)^2 + \cdots + (x_n - y_n)^2} \quad (12)$$

This equation is the ordinary l_2-metric on real coordinate space (R^n). In one dimension, i.e. n = 1, this equation gives the Euclidean line, in two dimensions, i.e. n = 2, the equation gives the Euclidean plane and in three dimensions when n = 3, the equation gives the Euclidean space. (Deza, Deza 2009.)

Essentially, in the case of spectral analysis the Euclidean distance equation can be expressed as follows:

$$d(x,y) = \sqrt{\sum_{i=1}^{n}(x_i - y_i)^2} \quad (13)$$

where x is the spectral signature vector of the sample [-]
y is the spectral signal vector of the reference [-]
n is the amount of wavelength bands [-]

The number of the wavelength bands is instrument dependent and a general rule is that the more image bands the instrument can measure, the more accurate information it gives. Generally, the equation calculates the length of the line segment between each corresponding wavelength band in the sample spectra and in the reference spectra. The difference of the intensity values on a given wavelength band is calculated and squared. All the differences in each wavelength band are then added together and a square root of the product is taken. The analysis is then continued by making the same calculations for each data point.

6.3.2 Classification of Reflectance Spectra

In this section, classification methods used specifically for data gained from reflectance spectroscopy are discussed. The data acquired with reflectance spectroscopy differed substantially from the data acquired with Raman spectroscopy. The target area covered by the light source in reflectance measurements was substantially larger than the area covered in Raman measurements. While the individual mineral grains could be easily measured with the laser source in Raman spectroscope, in reflectance measurements the separation could not be done due to the instrumentation used for the measurements. This meant that, in this research, the samples had to be analyzed as whole rather than specific areas within the samples, as is done with the Raman spectroscopy. Supervised machine learning and Pearson correlation coefficient were applied specifically for re-

flectance data. The following paragraphs describe the methods used for the classification in more detail.

The core principle behind supervised machine learning is to ”teach” computers to ”learn” to optimize a given performance criterion using available data. This “teaching” process is conducted via programming. In essence, supervised machine learning principles are based on pre-determined algorithms, with given parameters. These algorithms are implemented via computer program to optimize the said parameters using pre-existing data, i.e. to train a model. These models can be predictive or descriptive in nature. Predictive models make predictions on future observations based on the pre-existing data with which they are trained, and descriptive models attempt to gain more insight on existing data. (Alpaydin 2014.)

The theory of statistics is heavily implemented in machine learning models. This is due to the fact that the primary objective of these models is to make deductions based on sample data. Computer science plays two distinct roles in machine learning. The first role of computer science is related to model training. Computer science is needed to implement efficient algorithms to solve the specific optimization problem and to efficiently process large quantities of data, which would otherwise be highly time-consuming. The second role of computer science is to make sure that the algorithm used is efficient in its deduction process. In some instances, the deductive capabilities of the algorithm used in the model can be as crucial as the predictive accuracy of the model when applied to new data. (Alpaydin 2014.)

In this research, the supervised machine learning was first used to teach the computer to recognize different classes from a given training data using a given classification algorithm. After the training model was generated, it was cross-validated with 5-fold cross validation to generate the best possible model. The optimized model was then used on a new data set and the accuracy of predictions was evaluated.

For the analysis of reflectance spectroscopy data, three different sample sets were created for the supervised classification. The lower-grade samples were generally of much larger grain size than the medium-grade samples. However, some of the medium-grade samples had areas of more visible mineral crystals, i.e. larger grain size. The samples were divided into three distinct sample sets based on grain size information and the knowledge that grain size affects the hardness of the rock substantially. The first data set consisted of 60 training samples, the second of 50 and the third of 45 in total.

First of these sample sets consisted of a training set with 20 low-grade samples and 40 medium-grade samples. The medium-grade samples in this training set were of varying grain size, i.e. both large and fine grain size. The remaining 31 samples acted as a test set. The second sample set consisted of a training set with 20 low-grade and 30 medium-grade samples. All the medium-grade samples chosen for the training set were of a fine grain size. In this case, the remaining 41 samples acted as a test set. Finally, the last sample set consisted of a training set with 25 low-grade and 20 medium-grade samples. The medium-grade samples of this training set were of large grain size. The test set of the third sample set was comprised of 46 samples.

Several different classification algorithms were applied to all the sample sets to find the most accurate algorithms for each classification problem. The binary nature of the general classification problem was taken into account as well as the scarcity of the available

research data. After excessive testing and analysis, the conclusion was drawn that Supported Vector Machine or SVM proved to be the best classification algorithm for the available sample sets. Two applications of SVM were used, the first being Quadratic SVM and the second Cubic SVM.

The SVM has over the years established its position in supervised learning as one of the more powerful algorithms for classification problems. Many classification problems that in the past were mostly solved using neural networks have been found to be more efficient to solve using SVMs. SVMs also benefit from their relatively easy implementation and operation mechanics that are relatively easily understood. (William 2007.)

The problem of classification in supervised learning begins with a training data that consists of m data samples,

$$(x_i, y_i) \qquad i = 1, \dots, m \tag{14}$$

The x_i of a given sample is a so called feature vector describing the sample in n dimensions. Each corresponding y_i value ranges from -1 to 1, where the positive value indicates that the sample is included in the set that we want the computer to be able to learn to distinguish and negative value indicates that the sample is excluded from the set. What we need now is a decision rule or more specifically a decision function f(x). This function is implemented to predict the value of y, not only for the training set but also for new values of x. (William 2007.)

The concept of SVMs can be simplified as a series of generalizations from an ideal, often unrealistic, starting point. This starting point represents the ideal case where the data is completely linearly separable. In the ideal case, a hyperplane exists in n dimensions, which is essentially an n – 1 dimensional surface, and can be defined by the following equation:

$$f(x) = w * x + b = 0 \tag{15}$$

This surface completely separates the training data. This means that all the training samples with positive y_i lie on one side of the surface and the samples with negative y_i lie on the other side. To reach the decision rule f(x), we now have to find a normal vector, w, to the surface and an offset, b. (William 2007.) This decision rule summarizes the basic principle of SVM.

In the most common situation, more than one surface, or hyperplane, can separate linearly separable data. In this case we can consider the hyperplane with the largest margin. More specifically, we can consider the hyperplane that has the largest perpendicular distance to samples closest to the hyperplane on either side. In essence, no matter the hyperplane, its normal vector can always be scaled by a constant and the offset can be adjusted accordingly to achieve the following equations:

$$w * x_i + b \geq +1, \;\; when\; y_i = +1 \tag{16}$$
$$w * x_i + b \geq -1, \;\; when\; y_i = -1 \tag{17}$$

These equations serve as the hyperplanes that separate the samples on both sides of the decision function f(x), as illustrated in the figure 20. The perpendicular distance be-

tween the bounding hyperplanes can be easily analytically derived to be twice the margin illustrated in figure 20, more specifically:

$$2 * margin = 2(w * w)^{-\frac{1}{2}} \tag{18}$$

From this we can deduce that the maximum margin SVM, can be determined by solving a quadratic problem, where

$$w * w \tag{19}$$

is minimized, when being subjected to the following equation:

$$y_i(w * x_i + b) \geq 1, \quad i = 1, \ldots, m \tag{20}$$

The solution of the minimization must be so that a small portion of the samples lies exactly on the bounding hyperplanes. This is due to the fact that, if no samples lie on the bounding hyperplanes, the solution is not optimal and the margin between the bounding hyperplanes could have been made larger. This small portion of samples, which represent f(x) = ± 1, is referred to as support vectors, thus clarifying the term Support Vector Machines. Cubic SVM differs from the quadratic optimization problem in the fact that it uses a cubic polynomial to optimize the solution, instead of quadratic polynomial. (William 2007.)

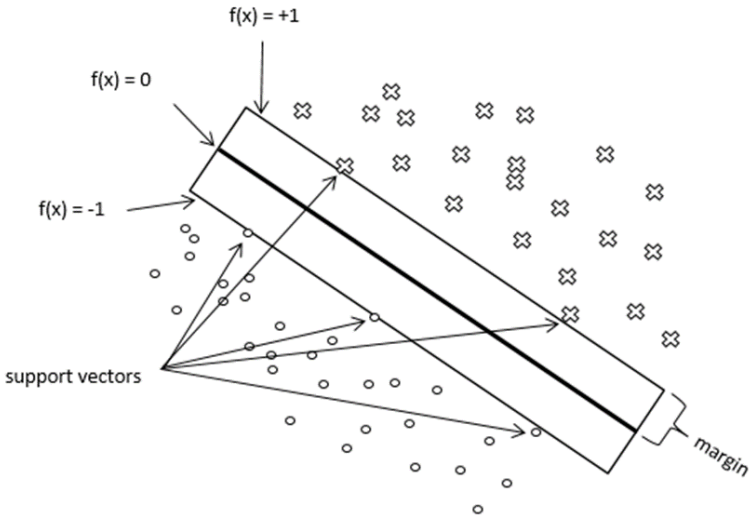

Figure 20. Illustration of Support Vector Machine in the case of linearly separable data. In this example, data containing crosses and circles is separated using the plane -1 ≤ f(x) ≤ 1. The goal is to maximize the margin shown in the figure. The data points that lie on the bounding planes f(x) = 1 and f(x) = -1, are referred to as the "support vectors". (Adapted from William 2007.)

The relationship between variables can be described by various statistics, but Pearson correlation coefficient is likely the most commonly used one. Pearson correlation coefficient is also referred to as the "product-moment correlation". This name comes from the computation of the Pearson correlation coefficient, which is done by first calculating the product of two examined variables and then calculating the moment of these products for a group of n instances. This means that variable X and Y are first assessed for these n instances. Subsequently, linear transformation equation is used to transform the standardized scores, z_{Xi} and z_{yi}, from the matching raw scores, X_i and Y_i, for a given instance i, as demonstrated in equations 21 and 22. (Chen, Popovich 2002.)

$$z_{Xi} = \frac{X_i - \bar{X}}{s_X} \tag{21}$$

$$z_{Yi} = \frac{Y_i - \bar{Y}}{s_Y} \tag{22}$$

where $\bar{X}$ is the mean of variable X [-]
$\bar{Y}$ is the mean of variable Y [-] (Chen, Popovich 2002).

The standard deviations s_X and s_Y of the variables X and Y are defined by the following equations:

$$s_X = \sqrt{\frac{\sum(X_i - \bar{X})^2}{n}} \tag{23}$$

$$s_X = \sqrt{\frac{\sum(X_i - \bar{X})^2}{n}} \tag{24}$$

Ultimately, all of this leads to the following formulation of Pearson correlation coefficient:

$$\frac{\sum(z_{Xi} x_{Yi})}{n} \tag{25}$$

The formulation of the Pearson correlation coefficient is the average of the sum of the standardized score product. The value of Pearson correlation coefficient ranges from -1 to 1, where -1 indicates a total negative linear correlation, 0 indicates no linear correlation and 1 indicates a total positive linear correlation. The Pearson correlation coefficient assumes symmetrical approach to both variables X and Y, meaning that the coefficient of X and Y is the same as the coefficient of Y and X. (Chen, Popovich 2002.) Usually, the correlation values exist somewhere between -1 and 0 or 0 and 1, with total correlations being very rare.

The standardized scores describe the position of each case i in relation to all of the n cases regarding variables X and Y. This is because the standardized scores, z_{Xi} and z_{Yi}, are for the most part determined by $(X_i - \bar{X})$ and $(Y_i - \bar{Y})$. In the case that a given sample has a high score on both variables, the outcome of both, $(X_i - \bar{X})$ and $(Y_i - \bar{Y})$, is large and positive. This also means that if a given sample scores low on both variables, it will subsequently acquire large standardized scores on both variables, also resulting in the outcome of $(X_i - \bar{X})$ and $(Y_i - \bar{Y})$ being large and positive. A positive relationship between variables X and Y occurs only if the average sum of all the products $(X_i - \bar{X})$ and $(Y_i - \bar{Y})$ is positive. This also means that if the average sum of the products is negative, the variables have a negative relationship, i.e. X is negatively related to Y. As an exam-

ple, a negative relationship may occur in a case where positive standardized scores of a given variable correspond with negative scores on a different variable. (Chen, Popovich 2002.)

6.3.3 Classification of Raman Spectra

As mentioned earlier, Raman spectroscopy allowed for a more in-depth analysis of the rock samples. This lead to the decision to use the most representative samples from both sample classes for in-depth mineral mapping analysis of the rock structure, and to an attempt to classify data points from the samples to recreate the sample structure using machine learning. It was hypothesized that if the different mineral areas could be identified from samples of interest, based on empirical knowledge of rock hardness, weak and strong areas could then be identified from the samples. In this section, the specific classification methods used for Raman spectroscopy, i.e. hierarchical cluster analysis is presented.

Hierarchical cluster analysis is generally classified as a method of unsupervised learning. The principle of unsupervised learning methods differ from supervised learning methods in that the unsupervised methods utilize algorithms to classify input data with no available training data with "correct answers", whereas supervised methods utilize training data to generate classification model. Essentially, cluster analysis seeks to cluster an unordered set of data into groups without any prior information about the data. As an output, hierarchical clustering algorithm presents distinct groups of data with different hierarchical levels. On the smallest of these levels are the individual data points, whereas on the largest of these levels is the whole data set itself. The data sets residing in between these levels are nested, meaning that either the null set or the smaller of two given sets acts as the intersection between the two sets. (William 2007.)

Cluster analysis was implemented for the data acquired from the Raman spectroscopy measurements with a goal to divide the data points into clear mineralogical groups. The form of clustering used in this research was agglomerative hierarchical clustering. Agglomerative hierarchical clustering could be used because the available data set was not too large. The basic principle of the agglomerative hierarchical clustering is to merge individual clusters when moving up the hierarchy. First each data point is divided into its own cluster, then based on the given distance metric similar elements are merged together to form the next level of hierarchy, i.e. new unified cluster. The distance between clusters grows after each agglomeration, or hierarchy level. The clustering process may be terminated based on the distance of the clusters or the number of the clusters. A specific distance restriction can be applied, after which the clustering process does not produce new clusters, or a desired number of created clusters can be specified when initiating the clustering process.

In this research, Euclidean distance was used as distance metric to calculate the cluster distances. The clustering criterion was specified to be the numbers of clusters, which was four, based on the reference mineral groups. Ward's method was specified as the method to divide the cluster tree into specific hierarchy levels.

The basic principle behind the Ward's clustering method is the minimization of a measure known as Ward distance. Ward distance describes the degree of disparity between

clusters, thus in agglomerative clustering, Ward's method aims to minimize the total variance within generated clusters. (Mirkin 2012.)

After hierarchical clustering, the components of the data, which contribute the most to the within-data variance, were determined using principal component analysis. Principal component analysis is a dimensional reduction method that aims to gather the essential information from multidimensional data without significant loss of characterizing information. The reduction of dimensions has a wide range of benefits in data analysis, some of them being the improved computational efficiency of the data and possible improvement in the performance of machine learning models.

Two components, which describe most of the data variance, were determined based on the principal component analysis. These components were then used in conjunction with the hierarchical cluster analysis to determine which reference groups the generated clusters represented. Once the clusters were labeled, a mineral map could be formulated based on the group labels of each of the data points. The formulated map was then visually compared to the measurement surface to assess the accuracy of the classification. This was possible because the minerals and their locations on the measurement surface were identified previously.

7 Results

In this chapter, results of the research methods are presented. The results are presented based on three different accuracy assessment methods. These methods are User's Accuracy, Producer's accuracy and Total Accuracy. All these methods assess the accuracy differently, with Total Accuracy being the average accuracy of the method. The User's Accuracy corresponds primarily to the error of inclusion, i.e. it describes the portion of samples that were erroneously classified to the given category. The Producer's accuracy, on the other hand, corresponds to the error of exclusion, i.e. the portion of samples that have not been classified correctly to their actual category. Essentially, the User's Accuracy describes the reliability of the results, whereas the Producer's accuracy describes the general accuracy of a given class.

The results are divided based on the instrumentation used. The different accuracies for each method are presented in individual tables with the total accuracy of each method located at the bottom right hand corner of each table. First, the section 8.1. focuses on the results of reflectance spectroscopy and lastly, the results of Raman spectroscopy are presented in section 8.2.

7.1 Classification of Reflectance Spectra

In this section, the results of the methods applied for reflectance spectroscopy data are presented. First, the results of physically-based spectral analysis methods are discussed. After the results of physically-based methods, the focus is directed towards the statistical classification methods. The first statistical classification methods to be presented are the machine learning algorithms, quadratic support vector machine and cubic support vector machine. Lastly, the results of the linear correlation method applied in this research, i.e. Pearson correlation coefficient, are presented.

7.1.1 Physically-Based Methods

As mentioned in previous chapters, the aim of physically-based methods was to assess the classification accuracy of two different spectral properties, spectral angle and Euclidean distance, when separating data into two distinct classes. The different accuracies are presented with tables and the overall accuracy of a specific method is described by the number located in the bottom right-hand corner of the table in question.

The results of the spectral angle mapper algorithm indicate that 39 of 57 (or 68 %) medium grade samples are classified correctly to the medium-grade class, whereas 18 of 57 (or 32 %) are classified falsely to the low-grade class. On the other hand, when classifying low-grade samples, the results indicate that 18 of 34 (or 53 %) samples are classified correctly to the low-grade class and 16 of 34 (or 47 %) samples are classified falsely to the medium-grade class. These results as well as the overall accuracies are illustrated in table 3.

Table 3. The accuracy of spectral angle mapper.

Predicted	Known				
	Medium-grade	Low-grade	Totals	User's (%)	Accuracy
Medium-grade	39	16	55	71	
Low-grade	18	18	36	50	
Totals	57	34	91		
Producer's Accuracy (%)	68	53		63	

The results of the Euclidean distance algorithm are in general, slightly less accurate than the results of the spectral angle mapper algorithm. When analyzing medium-grade samples, the algorithm classifies 34 of 57 (or 60 %) samples to medium-grade class and 23 of 57 (or 40 %) samples falsely to low-grade class. The error is slightly more pronounced in the analysis of low-grade samples, where the algorithm classifies only 16 of 34 (or 47 %) samples correctly to low-grade class, and 18 of 34 (or 53 %) samples falsely to medium-grade class. The results and overall accuracy are illustrated in table 4.

Table 4. The accuracy of Euclidean distance.

Predicted	Known				
	Medium-grade	Low-grade	Totals	User's (%)	Accuracy
Medium-grade	34	18	52	65	
Low-grade	23	16	39	41	
Totals	57	34	91		
Producer's Accuracy (%)	60	47		55	

Based on these results, spectral angle mapper has a slightly higher accuracy when evaluating the correct classification of all data. Generally, both of these models tend to classify a higher percentage of the data as medium-grade than as low-grade.

7.1.2 Statistical Classification Methods

Statistical classification methods used for reflectance spectroscopy data can be divided into two sections, machine learning methods and linear correlation method. Machine learning methods are significantly more complex of the two, and subsequently resulted in greater overall classification accuracy. The results of these methods are presented in the following paragraphs.

Three different sample sets were used for machine learning. Each of the sample sets comprised of different training and test sets based on different properties of the used rock samples. The primary focus in all of the sample sets were the samples of the medium-grade group, mainly due to the homogeneity within the low-grade group, i.e. the samples of low-grade group were generally of the same grain size and composition, whereas the samples of the medium-grade group sometimes had random areas of varying grain size. The composition of the medium-grade samples varied between the training sets, but in all of the test sets the composition of low-grade samples stayed constant.

The first sample set to be classified consisted of a set of 60 samples, which acted as the training set, and a set of 31 samples, which acted as the test set. Of the 60 samples included in the training set, more than half (namely 40) were medium-grade samples. These medium-grade samples were of varying grain size. The test set consisted of 17 medium-grade samples and 14 low-grade samples. The training accuracy of both classification algorithms, i.e. Quadratic SVM and Cubic SVM, are presented in tables 5 and 6. The final results of both algorithms, when applying to new data, are presented in tables 7 and 8. As can be seen from tables 7 and 8, both of the methods achieved exactly same accuracies when applied to new data.

Table 5. The training accuracy of Quadratic Support Vector Machine algorithm.

Predicted	Known				
	Medium-grade	Low-grade	Totals	User's (%)	Accuracy
Medium-grade	38	8	46	83	
Low-grade	2	12	14	86	
Totals	40	20	60		
Producer's Accuracy (%)	95	60		83	

Table 6. The training accuracy of Cubic Support Vector Machine algorithm.

Predicted	Known				
	Medium-grade	Low-grade	Totals	User's (%)	Accuracy
Medium-grade	35	7	42	83	
Low-grade	5	13	18	72	
Totals	40	20	60		
Producer's Accuracy (%)	88	65		80	

Table 7. The accuracy of Quadratic Support Vector Machine algorithm, when applied to new data.

Predicted	Known				
	Medium-grade	Low-grade	Totals	User's (%)	Accuracy
Medium-grade	17	6	23	74	
Low-grade	0	8	8	100	
Totals	17	14	31		
Producer's Accuracy (%)	100	57		81	

Table 8. The accuracy of Cubic Support Vector Machine algorithm, when applied to new data.

Predicted	Known				
	Medium-grade	Low-grade	Totals	User's (%)	Accuracy
Medium-grade	17	6	23	74	
Low-grade	0	8	8	100	
Totals	17	14	31		
Producer's Accuracy (%)	100	57		81	

The second analyzed sample set consisted of a training set of 50 samples and a test set of 41 samples. In this data set, the training set had a smaller percentage of medium-grade samples. The 30 medium-grade samples in the training set consisted only of samples with a small grain size, thus in this sample set, the medium-grade group and low-grade group had the largest margin separating each other. The training accuracies of Quadratic SVM and Cubic SVM are presented in tables 9 and 10.

Table 9. The training accuracy of Quadratic Support Vector Machine algorithm for data set 2.

Predicted	Known				
	Medium-grade	Low-grade	Totals	User's (%)	Accuracy
Medium-grade	26	8	34	76	
Low-grade	4	12	16	75	
Totals	30	20	50		
Producer's Accuracy (%)	87	60		76	

Table 10. The training accuracy of Cubic Support Vector Machine algorithm for data set 2.

Predicted	Known				
	Medium-grade	Low-grade	Totals	User's (%)	Accuracy
Medium-grade	25	9	34	74	
Low-grade	5	11	16	69	
Totals	30	20	50		
Producer's Accuracy (%)	83	55		72	

The accuracies when applying to new data are presented in tables 11 and 12. It is worth mentioning that with this data set, even though Cubic SVM algorithm had a lower training accuracy, during the classification of new data it was able to reach significantly higher classification accuracy.

Table 11. The classification accuracy of Quadratic Support Vector Machine algorithm for data set 2.

Predicted	Known			
	Medium-grade	Low-grade	Totals	User's Accuracy (%)
Medium-grade	23	5	28	82
Low-grade	4	9	13	69
Totals	27	14	41	
Producer's Accuracy (%)	85	64		78

Table 12. The classification accuracy of Cubic Support Vector Machine algorithm for data set 2.

Predicted	Known			
	Medium-grade	Low-grade	Totals	User's Accuracy (%)
Medium-grade	24	3	27	89
Low-grade	3	11	14	79
Totals	27	14	41	
Producer's Accuracy (%)	89	79		85

The third and final sample set consisted of a training set with 45 samples and a test set of 46 samples. The percentage of low-grade samples in the training set of this data set was higher than the percentage of medium-grade samples and the medium-grade samples consisted only of the samples with areas of noticeably larger grain size. This means that the medium-grade group and low-grade group had the smallest margin separating the classes. The training performances of the classification algorithms are presented in tables 13 and 14. It is worth mentioning that this was the only sample set where the Cubic SVM algorithm outperformed the Quadratic SVM algorithm in training.

Table 13. The training accuracy of Quadratic Support Vector Machine Algorithm for data set 3.

Predicted	Known			
	Medium-grade	Low-grade	Totals	User's Accuracy (%)
Medium-grade	13	5	18	72
Low-grade	7	20	27	74
Totals	20	25	45	
Producer's Accuracy (%)	65	80		73

Table 14. The training accuracy of Cubic Support Vector Machine algorithm for data set 3.

Predicted	Known				
	Medium-grade	Low-grade	Totals	User's (%)	Accuracy
Medium-grade	15	2	17	88	
Low-grade	5	23	28	82	
Totals	20	25	45		
Producer's Accuracy (%)	75	92		84	

When the trained models were applied to new data, Cubic SVM algorithm performed significantly better, proving to be the only case where the more accurate training algorithm was also significantly more accurate in classification of new data. The results of both algorithms are presented in tables 15 and 16.

Table 15. The classification accuracy of Quadratic Support Vector Machine for data set 3.

Predicted	Known				
	Medium-grade	Low-grade	Totals	User's (%)	Accuracy
Medium-grade	23	4	27	85	
Low-grade	14	5	19	26	
Totals	37	9	46		
Producer's Accuracy (%)	62	56		61	

Table 16. The classification accuracy of Cubic Support Vector Machine for data set 3.

Predicted	Known				
	Medium-grade	Low-grade	Totals	User's (%)	Accuracy
Medium-grade	27	2	29	93	
Low-grade	10	7	17	41	
Totals	37	9	46		
Producer's Accuracy (%)	73	78		74	

Pearson correlation coefficient proved to be significantly less accurate than the machine learning methods in classification of reflectance data. High positive correlation between a class mean and a sample was used as the measure, with which the samples were classified to specific class, e.g. if a medium-grade sample had a higher positive correlation with the mean of the medium-grade class, than with the mean of the low-grade class, the sample was classified as medium-grade.

The correlations between the class means and the individual samples were generally of relatively high magnitude. The average correlation between medium-grade samples and the medium-grade class mean was 0.696, with the average correlation between medium-grade samples and low-grade class mean being 0.632. The average correlation between

the opposite classes was slightly higher when comparing low-grade samples and medium-grade class mean at 0.651, whereas the average correlation was slightly lower when comparing inside the same class, i.e. the average correlation between low-grade samples and low-grade class mean was at 0.674. The classification accuracy of Pearson correlation coefficient is presented in table 17.

Table 17. Classification accuracy of Pearson correlation coefficient. Percentages indicate the quantity of the known samples classified to given class based on the higher positive correlation.

Predicted	Known				
	Medium-grade	Low-grade	Totals	User's (%)	Accuracy
Medium-grade	37	15	52	71	
Low-grade	20	19	39	49	
Totals	57	34	91		
Producer's Accuracy (%)	65	56		62	

7.2 Classification of Raman Spectra

In this section, the results of the Raman spectroscopy data classification are presented. First, the focus is given to physically-based classification, and the results of the two classification algorithms are presented. Lastly, the results of the statistical classification, or more precisely the unsupervised machine learning methods, are presented. Unsupervised machine learning methods were used because the goal was to evaluate the capabilities of the algorithms in classification of data points with no previous training.

A key indicator of the success of classification was the presence of almandine in the computer generated model. Clear areas of almandine can be observed from the low-grade sample, as illustrated in the results**,** and these areas were expected to be clearly represented in the computer generated model due to the clear mineralogical differences in the constitution of the sample. The area with high almandine presence also contains a particularly interesting quartz inclusion (shown in appendix 2) that complicates the classification, thus it was highly crucial that the classification algorithm could differentiate the quartz grain from the surrounding almandine.

The results of the physically-based methods are presented in the following section 8.2.1 and finally, the results of the statistical methods are presented in section 8.2.2.

7.2.1 Physically-Based Methods

The results of the physically-based classification were generally much worse than the results of statistical classification. The physically-based algorithms varied slightly in performance, with Euclidean distance algorithm performing slightly better in both the classification of the medium-grade sample and the low-grade sample. Classification of data points of the low-grade sample exhibited the greatest variance between methods, while the classification of the medium-grade sample exhibited only minor misclassification of data points between methods. The results of the physically-based methods gen-

erally followed the structural orientation of the samples relatively well but problems surfaced, when data points needed to be classified to the specific mineral groups.

The results of the classification of the low-grade sample are presented in figures 21 and 22, with the appearance of the actual sample surface. The distinct mineral areas of the sample surface are presented more clearly in appendix 2. The figures clearly illustrate a fundamental problem in the physically-based classification, where iron rich biotite dominates the area of the surface that should be classified as k-feldspar, and the areas that should be classified as quartz are in turn classified as k-feldspar. All in all, quartz suffers a complete lack of presence in the model, with only one data point in the spectral angle mapper classification, and only a few in the Euclidean distance classification classified as quartz.

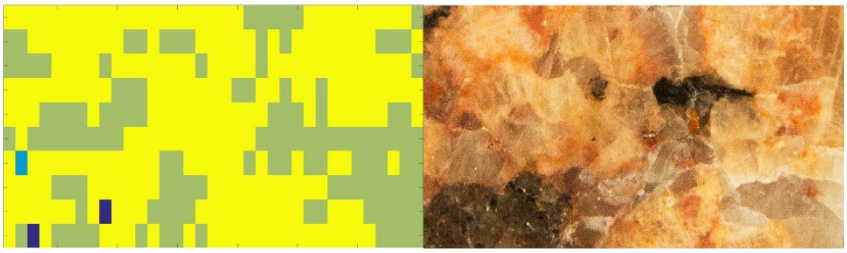

Figure 21. The results of the Spectral Angle Mapper algorithm compared to the actual sample surface. The colors of the classification map represent the following minerals; almandine (purple), quartz (blue), k-feldspar (green), and biotite (yellow).

Figure 22. The results of the Euclidean distance algorithm compared to the actual sample surface. The colors of the classification map represent the following minerals; almandine (purple), quartz (blue), k-feldspar (green), and biotite (yellow).

The structural orientation of the samples is followed quite well in the model, even though the classification is completely false. The medium-grade sample models, based on the classification algorithms, are presented in figures 23 and 24, again with the actual sample surface. The mineral areas of the actual sample are presented in appendix 2.

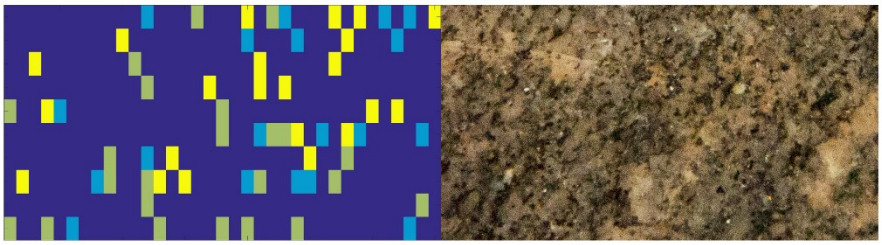

Figure 23. The results of the Spectral Angle Mapper algorithm compared to the actual sample surface. The colors of the classification map represent the following minerals; anorthite (purple), quartz (blue), k-feldspar (green), and biotite (yellow).

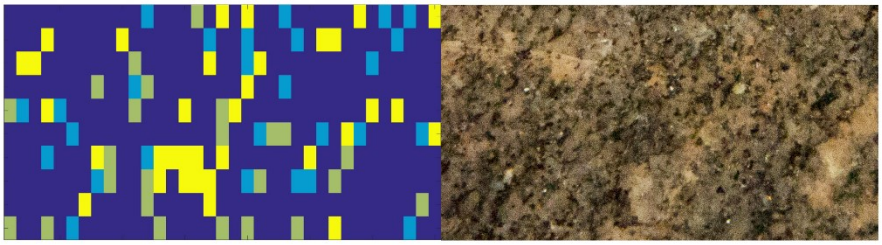

Figure 24. The results of the Euclidean distance algorithm compared to the actual sample surface. The colors of the classification map represent the following minerals; anorthite (purple), quartz (blue), k-feldspar (green), and biotite (yellow).

7.2.2 Statistical Classification Methods

As mentioned previously, statistical classification methods performed significantly better than the physically-based classification methods. The hierarchical agglomerative clustering combined with principal component analysis, was able to model the structure and mineral composition of the samples with relatively good precision, although some errors was experienced in classification of random data points.

Overall, the classification of data points to specific mineral groups was relatively successful, compared to physically-based algorithms, moreover the statistical classification was able to clearly distinguish the almandine area in the low-grade sample. The statistical classification was even able to distinguish the isolated quartz grain in the almandine formation.

Slightly different mineral references were used in the classification of the samples, based on the observed and documented mineral composition. While the low-grade sample was easy to analyze based on the relatively large mineral grains, the higher grade sample was finer in grain size and thus the minerals were harder to differentiate. The results of the statistical classification, along with the specific mineral references used, are presented in figures 25 and 26. The figures are presented with the actual sample surface, with appendix 2 describing the mineral areas of the actual sample.

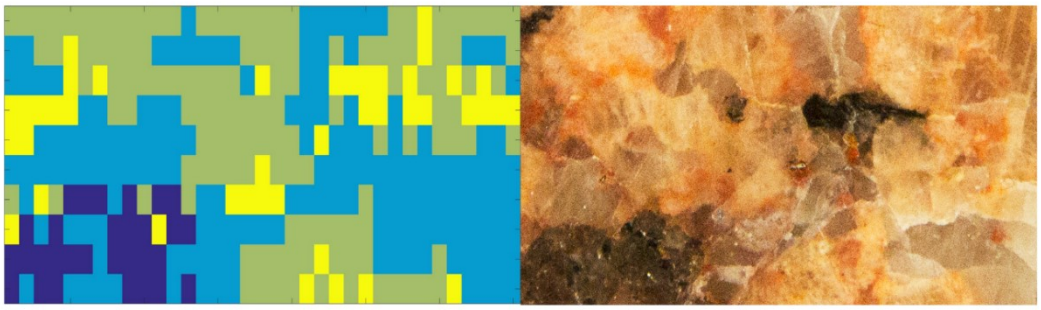

Figure 25. The results of hierarchical cluster and PCA classification for low grade sample. The colors of the classification map represent the following minerals; almandine (purple), quartz (blue), k-feldspar (green), and biotite (yellow).

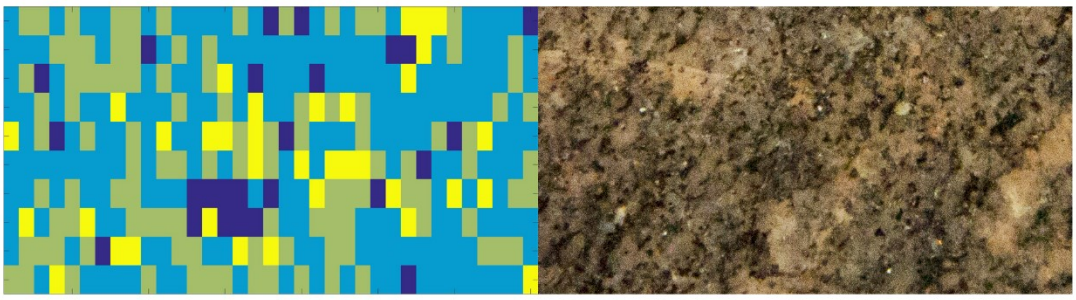

Figure 26. The results of hierarchical cluster and PCA classification for low grade sample. The colors of the classification map represent the following minerals; biotite (purple), quartz (blue), k-feldspar (green), and anorthite (yellow).

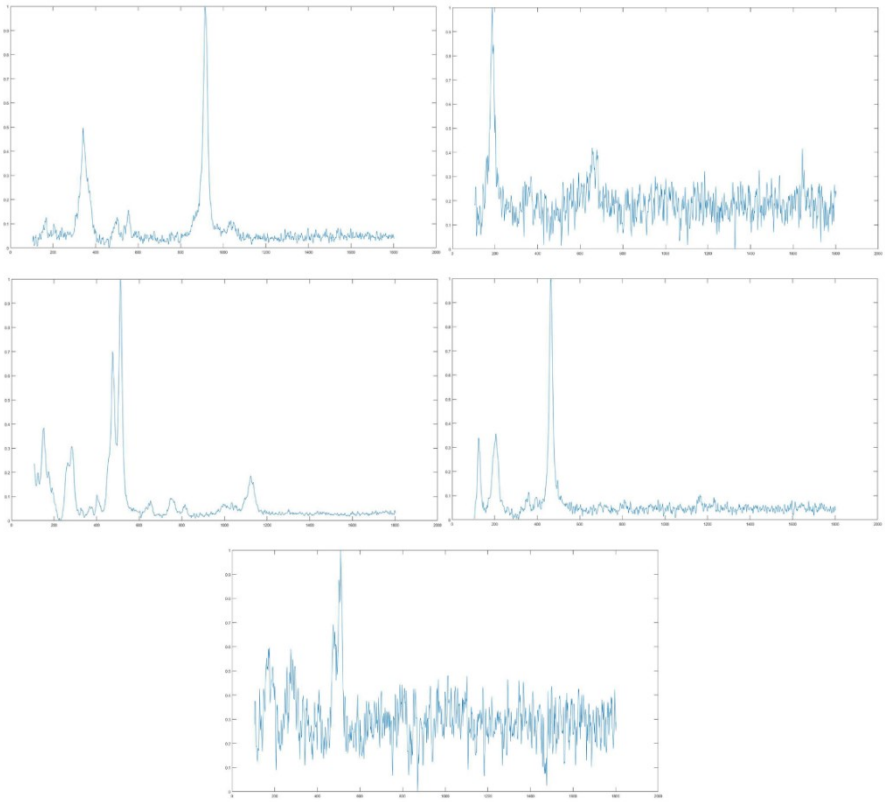

Figure 27. Reference spectra used for Raman classification. Upper row from left represents almandine and iron rich biotite, and middle row from left represents k-feldspar and quartz. The bottom row represents anorthite.

8 Discussion

This research concentrated on the possible relation between spectral information and the hardness of rock samples. It was researched whether it was possible to allocate given rock samples to specific groups based on the spectral data gathered with different methods. These different classification methods were applied with the intention to find the best solution that could reliably classify the samples.

The used measurement techniques clearly demonstrated the capabilities of spectral methods in classification of the samples of interest. A more intense, point-like light source can quite effectively be used in sample mapping, whereas a broader light source can be used to analyze larger surface areas.

The data gathered with the reflectance spectroscopy represented the analysis of larger surface areas. In general, the available data was slightly biased due to the larger content of higher grade samples in relation to lower grade samples. This bias was taken into account in the machine learning approach, where multiple data sets where formulated based on the known properties of the samples. The goal was to control the variance of the samples by making different sample sets, each with their own training and test sets. No such distinction was made in the case of physically-based analysis, nor the Pearson correlation coefficient analysis, because the data in these cases was always compared to the means of the two different classes.

In general, the best results in reflectance spectroscopy analysis were achieved using machine learning algorithms. The varying compositions of analyzed sample sets created variance in the classification accuracy, as one would expect. The algorithms used for the machine learning classification performed relatively well, with a significant drop in accuracy in only one data set. This data set consisted of a training set with the largest percentage of lower grade samples, with the sample distribution being namely 44 percent higher grade samples and 56 percent lower grade samples. On the other hand, the general accuracy was the highest in the data set where the percentage of higher grade samples in the training set was not the largest, namely 60 percent higher grade samples and 40 percent lower grade samples, but had the greatest variance between the sample groups, i.e. the higher grade samples were of the finest grain size.

The composition of the samples in both classes differed greatly from each other, with medium-grade samples being relatively fine grained and low-grade samples being significantly larger grained. This clear distinction in composition should allow the algorithms to classify the samples to the correct classes with relatively great precision, but this is not always the case, as can be seen from the results. It can be argued that the large grain size of the low-grade samples causes problems with the analysis because some of the large grains are likened to the higher grade samples and thus are interpreted as higher grade sample. This problem is more proficient in the reflectance spectroscopy measurements conducted in this research, because the light source of the setup illuminated such a large area of the measurement scene, compared to the light source of the Raman spectroscopy setup. The accuracy may also be affected to a degree by the angle in which the light hit the measurement scene. Because the reflectance measurements were conducted with the samples in their most natural state, the mineral grains were not always aligned perfectly perpendicular to the light source.

The training sets of the machine learning analysis not only differed in the amount of low-grade and medium-grade samples, but also in the composition of the medium-grade samples. The sample set that achieved the lowest accuracy of all the implemented sample sets, had a training set with not only the largest percentage of lower grade samples, but the higher grade samples also consisted of samples on the larger side of the grain size spectrum, i.e. the samples possessed larger grain size than the average of the medium-grade class. This introduces an idea that some of the higher grade samples in the test set were misclassified as lower grade samples because the training had misinterpreted some of the larger grained higher grade samples as lower grade samples.

The sample set that achieved the highest accuracy when the trained model was applied to test data was the data set which had the training set with the most margin between the sample groups. When the higher grade samples of the training set consisted only of samples on the fine side of the grain size spectrum, the cubic support vector machine algorithm was able to achieve a testing accuracy of 85 percent. It is worth noting that the training accuracy of the cubic SVM algorithm was lower than that of the quadratic SVM algorithm in this data set, but the cubic algorithm still achieved higher testing accuracy. This seems to suggest that the higher training accuracy is not always indicative of the model performance when applied to new data. Interesting aspect to also take note of is the fact that the training accuracy tends to decrease significantly with the quadratic SVM algorithm, when the percentage of the lower grade samples is increased, but the training accuracy of the cubic SVM algorithm reaches its highest value when the percentage of lower grade samples is the highest.

The Raman spectroscopy performed the role of the mapping analysis, ultimately with promising results. The intense laser light source enabled the analysis of specific mineral grains in the structure of the sample rock and thus different structural areas could be efficiently separated. Efficient mapping analysis could not be done using physically-based analysis, largely due to the fact that the captured mineral spectra was seldom pure and exhibited differences only in specific wavelengths with most of the spectral area being relatively similar in all of the measured points. The impure spectra also meant that it contained a lot of unnecessary characteristics, which contributed negatively to the accuracy of classification by blurring the clear physical differences between the spectra. These facts made the analysis of spectral angle and distance difficult.

On the other hand, cluster analysis together with principal component analysis, performed significantly better. When principal component analysis was performed on the data, and the components that explained most of the data variance were gathered, the cluster analysis was able to effectively separate the data into a desired number of clusters. The principal component analysis was essential in weeding out the undesirable nuances in the data that could not be eliminated in the physically-based analysis. Because the principal component analysis enabled the analysis of only the most significant differences in the data, the classification of point data was much more efficient.

The statistical classification of the Raman data is not without its faults and the success of the point data mapping is hard to assess, partly due to the nature of unsupervised learning algorithms. It can be seen however that the patterns formed by the statistical classification seem to follow the real mineral patterns in the samples and this clearly demonstrates the potential of Raman spectroscopy as a mineralogical mapping tool. On top of this, the statistical classification was relatively accurate in mapping the grain size composition of the different samples, with the mineral map of medium-grade sample

showing distinctly finer textures than that of the low-grade sample. The most challenging aspect in the point mapping is the application of the reference data to real life objects. The spectra of terrestrial materials are seldom pure, which creates challenges in the classification.

As mentioned before, in the case of Raman spectroscopy classification, machine learning algorithms were superior to other implemented methods. The machine learning algorithms were able to quite efficiently separate the measured data points from each other and classify them into specific mineral groups. The successful classification with machine learning was relatively high even in adjacent data points, when compared to physically-based algorithms which often classified adjacent data points to one general group. This general classification often left out important variations in the sample structure. One clear example of this generalization of classification is the almandine presence in the measured scene of the low-grade sample. While the machine learning algorithms could clearly differentiate the areas of almandine and even the quartz grains singled out by the almandine formation, the physically-based algorithms could only at best classify random measurement points as almandine and had trouble differentiate areas that were clearly mineralogically different.

The difference in classification accuracy can be attributed to not only the complexity of the classification algorithms, but also to the nature of the spectra derived from natural substances and objects, in this case rocks that are formed by minerals. These minerals seldom appear in their purest form in the nature. This can pose problems for the classification accuracy by diminishing the differences in the spectral signatures of objects of interest, but it would seem that this issue can be somewhat avoided by using algorithms with high enough complexity.

The Pearson correlation coefficient performed the classification with approximately the same accuracy as the physically based methods. Pearson correlation coefficient is also fairly simple classification method due to its linear nature, and can be fairly dependent on the data distribution. All of the samples exhibited positive correlation towards both mean of the medium-grade samples and mean of the low-grade samples, but generally medium-grade samples exhibited greater positive correlation towards the mean of their own class, and low-grade samples towards their own class. The positive correlations can be attributed to the nature of spectral data, and the fact that only substantial difference between the sample classes was the variation in grain size and brightness of grains. Despite this, the Pearson correlation coefficient is able to classify the samples correctly with mediocre accuracy. This is perhaps due to the difference in intensity between the samples of medium-grade class and low-grade class, with the brighter lower-grade samples having generally greater intensities than the medium-grade samples.

If we take a look at the average User's and Producer's accuracies of all the classification methods, we can see that for the physically based methods, spectral angle mapper and Euclidean distance, both of these accuracies are 60 percent and 50 percent, respectively. For Pearson's correlation coefficient, these accuracies are both 60 percent. The machine learning methods indicate a clear improvement in both User's and Producer's accuracy, with only one relatively weak classification. This weak classification was performed with quadratic SVM algorithm for the third sample set, and the achieved accuracies for User's and Producer's accuracies were 55 and 60 percent respectively. The first sample set achieved User's accuracy of 90 percent and Producer's accuracy of 80 percent for both algorithms. For the second set, the quadratic algorithm achieved accuracies of 75

percent, and the cubic algorithm accuracies of 85 percent. The cubic algorithm for the third sample set achieved User's accuracy of 70 percent and Producer's accuracy of 75 percent. These parameters clearly demonstrate that the cubic algorithm is the superior among the machine learning methods for infrared, or reflectance, spectroscopy.

All in all, the physically based classification methods, as well as Pearson correlation coefficient, performed significantly worse than the machine learning based statistical classification methods for both the Raman spectroscopy and infrared spectroscopy. Based on the results of this study, physically based algorithms have a tendency to classify larger portions of samples towards the data which consists of samples with finer grain sizes. The fine grained samples are also the samples that are darker in color and thus the intensities of their reflectance spectra is lower than the intensities of the more brighter colored, larger grained samples. Supervised statistical classification is largely dependent on the training samples and the formulation of the training sets with which the classification models are created. Large sample sets would be needed for an ideal training set to be generated, and one of the restricting factors in this research was the relatively low number of samples. Unsupervised learning methods used in this research are highly robust due to the use of principal component analysis, but are still largely dependent on clear and precise spectra for accurate differentiation of clusters.

9 Conclusions

The basis of this research was the idea that rock samples could be differentiated using spectroscopy. The main research aspects were the general success of spectroscopic methods, the assessment of the most successful classification method, and the possibility of applying the given methods to field conditions.

The research clearly demonstrated that rock samples of different hardness can be classified using spectroscopy, with the best methods achieving overall accuracies of 80 % and above, but the success of the classification is largely dependent on the algorithms used to perform the classification. A general conclusion was reached that the more complex the algorithm, the more accurate it was when performing the classification. This conclusion concerns only the samples used in this study and cannot yet be viably generalized. This lead to the assessment that the algorithms that examined the physical properties of spectral data were inferior to the algorithms that used statistics of the sample groups to formulate a classification model. The reliability of classification results and the accuracy of the classification were both generally higher in statistics based classification, as seen from the User's and Producer's Accuracies presented in the chapter 8.

Overall, the most successful classification method for infrared spectroscopy was concluded to be the cubic polynomial function for the support vector machine algorithm, and the most successful method for the Raman spectroscopy was concluded to be the agglomerative hierarchical clustering.

The field application of these techniques would be possible with an extensive reference library and knowledge of geology. Reference library is essential for the success of the statistical classification, because the models have to be taught to separate data, and the knowledge of geology is needed for the pre-evaluation of the area of study. Infrared spectroscopy has already been verified as a potential industrial technique in the past, and both of the techniques benefit from their non-destructive nature and minimal sample preparation.

Ultimately, the results of this study indicate that there are correlations between the spectral properties of rocks and their hardness, and because the hardness of a rock is largely dependent on the grain size and mineral composition, it can be concluded that the spectroscopic techniques can be applied to mineralogical materials to assess their structure and suitability to construction purposes.

Bibliography

ALPAYDIN, E., 2014. *Introduction to machine learning.* MIT press.

BOKOBZA, L., 1998. Near infrared spectroscopy. *Journal of Near Infrared Spectroscopy,* **6**, pp. 3-18.

BURNS, R.G., 1993. *Mineralogical applications of crystal field theory.* Cambridge University Press.

CHEN, P.Y. and POPOVICH, P.M., 2002. *Correlation: Parametric and nonparametric measures.* Sage.

CHESNER, W.H. and MCMILLAN, N.J., 2012. *Automated Laser Spectrographic Pattern Matching for Aggregate Identification.* 1. Washington, USA: Transportation Research Board of the National Academies.

CLARK, R.N., 1995. *Reflectance Spectra, in Rock Physics & Phase Relations: A Handbook of Physical Constants.* 1 edn. Washington, D. C.: American Geophysical Union.

DE CARVALHO, O.A. and MENESES, P.R., 2000. Spectral correlation mapper (SCM): an improvement on the spectral angle mapper (SAM), *Summaries of the 9th JPL Airborne Earth Science Workshop, JPL Publication 00-18* 2000, JPL Publication Pasadena, CA.

DE VALLEJO, LUIS I GONZÁLEZ and FERRER, M., 2011. *Geological engineering.* CRC Press.

DEZA, M.M. and DEZA, E., 2009. Encyclopedia of distances. *Encyclopedia of Distances.* Springer, pp. 1-583.

DORÉ, G. and ZUBECK, H.K., 2009. *Cold regions pavement engineering.*

EISMANN, M.T., 2012. Hyperspectral remote sensing, 2012, SPIE Bellingham.

FARMER, V., 1998. Differing effects of particle size and in the infrared and Raman spectra kaolinite shape. *Clay Minerals,* **33**(4), pp. 601-604.

GARDEMEISTER, R., KAURANNE, L.K., KORPELA, K. and MÄLKKI, E., 1972. *Rakennegeologia II 304.* 2 edn. Espoo: Otakustannus.

GEOLOGICAL SURVEY OF FINLAND, GTK. <hakku.gtk.fi>. 10.11.2014.

HUBBARD, A.T., 1995. *The Handbook of surface imaging and visualization.* CRC Press.

HUNT, G.R., 1977. Spectral signatures of particulate minerals in the visible and near infrared. *Geophysics,* **42**(3), pp. 501-513.

LEHTINEN, M., NURMI, P.A. and RÄMÖ, T., 1998a. *Suomen kallioperä: 3000 vuosimiljoonaa.*

LEHTINEN, M., NURMI, P.A. and RÄMÖ, T., 1998b. *Suomen kallioperä: 3000 vuosimiljoonaa.*

LOUDON, R., 1965. Theory of the resonance Raman effect in crystals. *Journal de Physique,* **26**(11), pp. 677-683.

MIRKIN, B., 2012. *Clustering: a data recovery approach.* CRC Press.

NURMIKOLU, A., 2004. *Murskatun kalliokiviaineksen hienoneminen ja routivuus radan rakennekerroksissa.* Helsinki: Ratahallintokeskus.

PENNER, M.H., 2010. Basic principles of spectroscopy. *Food Analysis.* Springer, pp. 375-385.

PIDWIRNY, M. 2006. Introduction to Geography. *Fundamentals of Physical Geography.* 2nd edition. University of British Columbia.

RANDOLPH, T.W., 2006. Scale-based normalization of spectral data. *Cancer Biomarkers,* **2**(3-4), pp. 135-144.

RIAZA, A., STROBL, P., BEISL, U., HAUSOLD, A. and MÜLLER, A., 2001. Spectral mapping of rock weathering degrees on granite using hyperspectral DAIS 7915 Spectrometer Data. *International Journal of Applied Earth Observation and Geoinformation,* **3**(4), pp. 345-354.

SCHRADER, B., BOUGEARD, D., BUBACK, M. and CAO, A., 1995. Infrared and Raman spectroscopy: methods and applications.

SFS-EN 1097-2. 2010. *Tests for mechanical and physical properties of aggregates. Part 2: Methods for the determination of resistance to fragmentation.* 2 edn. Helsinki: Finnish standards association SFS.

SFS-EN 1097-9. 2014. *Tests for mechanical and physical properties of aggregates. Part 9: Determination of the resistance to wear by abrasion from studded tyres.* 2 edn. Helsinki: Finnish standards association SFS.

SFS-EN 13043. 2002. *Aggregates for bituminous mixtures and surface treatments for roads, airfields and other trafficked areas.* Helsinki: Finnish standards association SFS.

SFS-EN ISO 14689-1:2003. 2004. *Geotechnical investigation and testing. Identification and classification of rock. Part 1: Identification and description.* Helsinki: Finnish standards association SFS.

SIESLER, H.W., OZAKI, Y., KAWATA, S. and HEISE, H.M., 2008. *Near-infrared spectroscopy: principles, instruments, applications.* John Wiley & Sons.

STUART, B., 2005. *Infrared spectroscopy.* Wiley Online Library.

VAN DER MEER, F., 2004. Analysis of spectral absorption features in hyperspectral imagery. *International journal of applied earth observation and geoinformation,* **5**(1), pp. 55-68.

WILLIAM, H., 2007. Press. Numerical recipes 3rd edition: The art of scientific computing.

YOUNG, H.D. and FREEDMAN, R.A., 2004. University physics with modern physics.

Appendices

Appendix 1. Raman samples. 2 pages.
Appendix 2. Mineral areas of the Raman sample surfaces. 2 pages.

Appendix 1. Raman samples.

Sample 1. The sample with the superior hardness grade.

Sample 2. The sample with the inferior hardness grade.

Appendix 2. Mineral areas of the Raman sample surfaces.

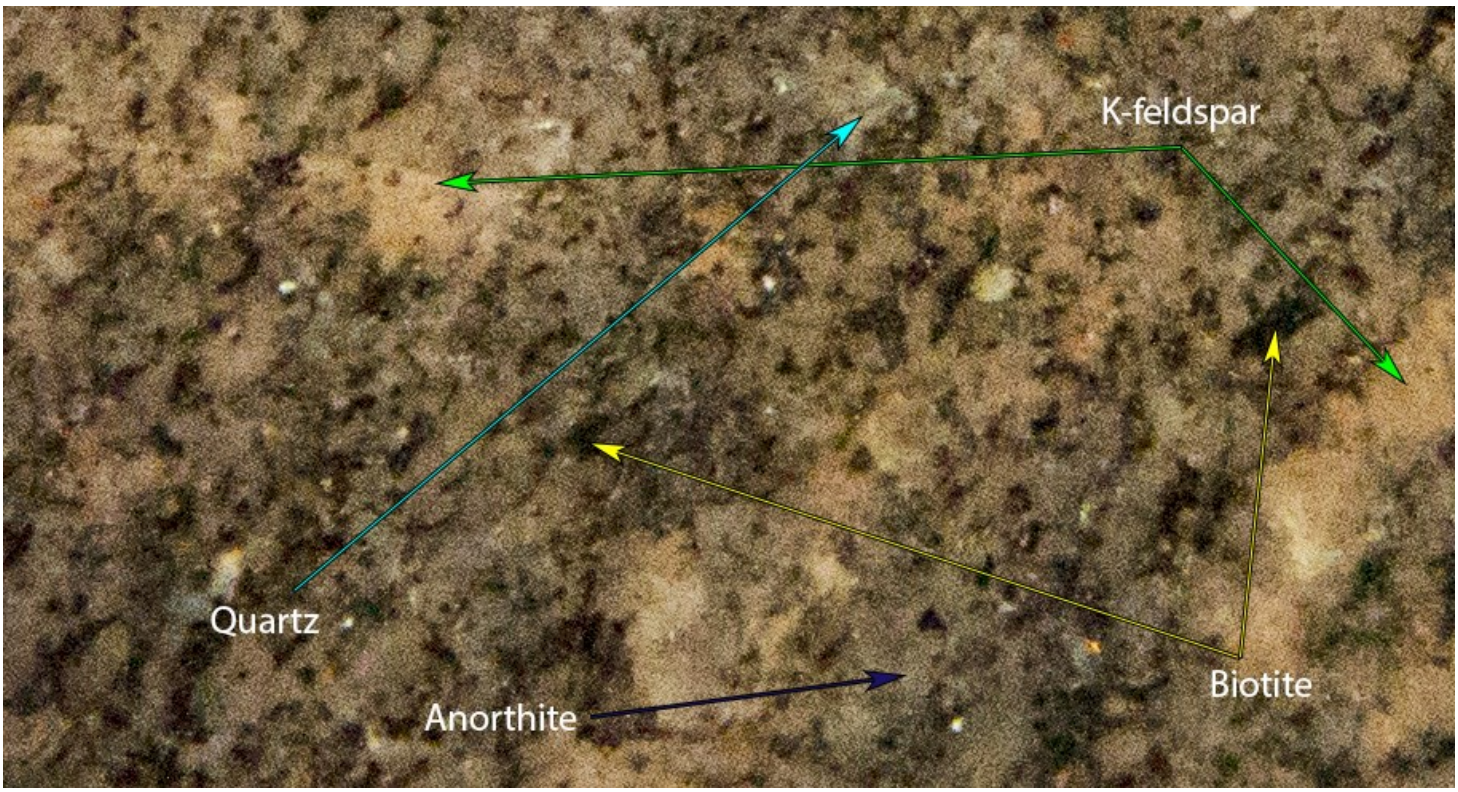

Sample 1. Mineral areas of the superior grade sample surface.

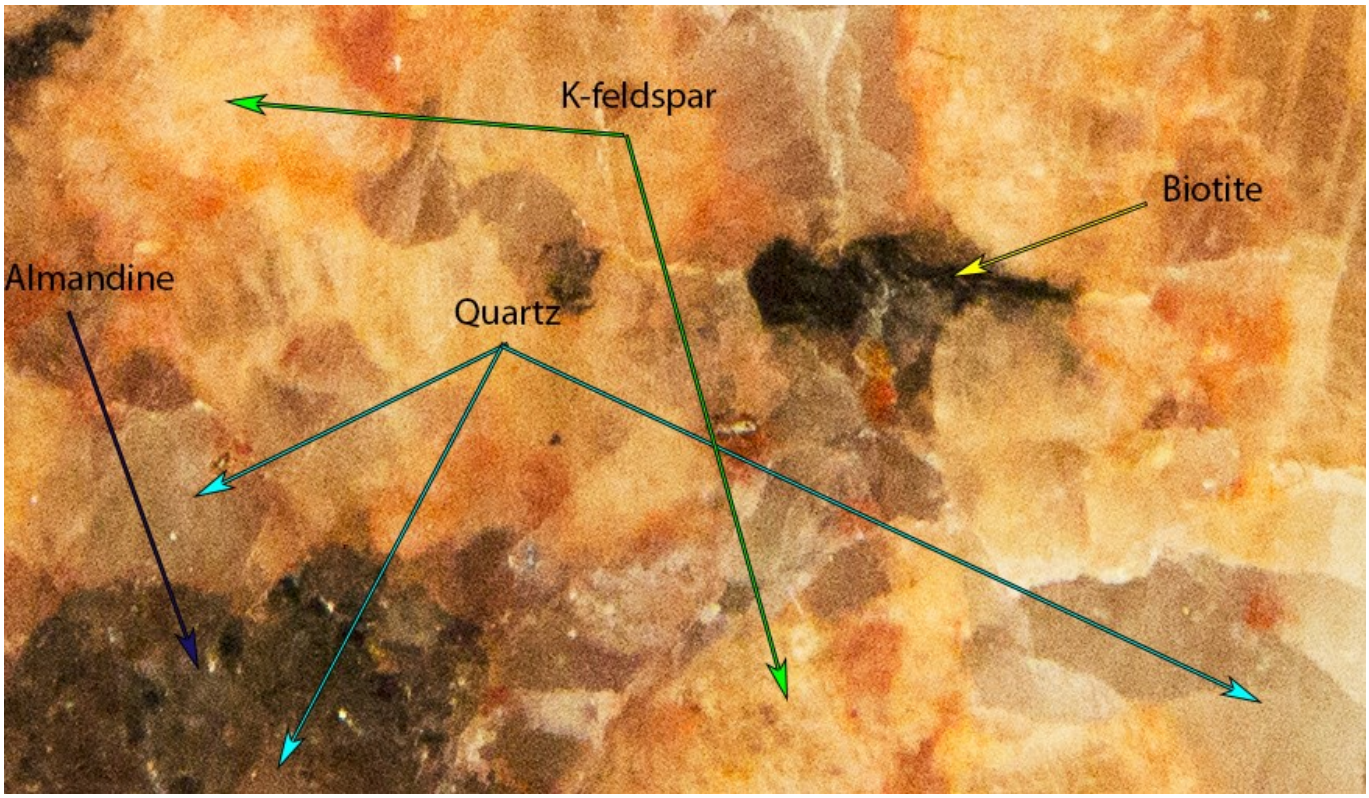

Sample 2. Mineral areas of the inferior grade sample.